

Entanglement transitions in a periodically driven non-Hermitian Ising chain

Tista Banerjee and K. Sengupta

School of Physical Sciences, Indian Association for the Cultivation of Science, Jadavpur, Kolkata 700032, India.

(Dated: October 5, 2023)

We study entanglement transitions in a periodically driven Ising chain in the presence of an imaginary transverse field γ as a function of drive frequency ω_D . In the high drive amplitude and frequency regime, we find a critical value $\gamma = \gamma_c$ below which the steady state half-chain entanglement entropy, $S_{L/2}$, scales with chain length L as $S_{L/2} \sim \ln L$; in contrast, for $\gamma > \gamma_c$, it becomes independent of L . In the small γ limit, we compute the coefficient, α , of the $\ln L$ term analytically using a Floquet perturbation theory and trace its origin to the presence of Fisher-Hartwig jump singularities in the correlation function of the driven chain. We also study the frequency dependence of γ_c and show that $\gamma_c \rightarrow 0$ at special drive frequencies; at these frequencies, which we analytically compute, $S_{L/2}$ remain independent of L for all γ . This behavior can be traced to an approximate emergent symmetry of the Floquet Hamiltonian at these drive frequencies which we identify. Finally, we discuss the behavior of the driven system at low and intermediate drive frequencies. Our analysis shows the presence of volume law behavior of the entanglement in this regime $S_\ell \sim \ell$ for small subsystem length $\ell \leq \ell^*(\omega_D)$. We identify $\ell^*(\omega_D)$ and tie its existence to the effective long-range nature of the Floquet Hamiltonian of the driven chain for small subsystem size. We discuss the applicability of our results to other integrable non-hermitian models.

PACS numbers:

I. INTRODUCTION

Entanglement is a key feature of quantum many-body systems¹⁻⁶. Its properties lead to important information about nature of many-body quantum states. For example, it is expected that a reduced density matrix ρ_{red} constructed from the ground state (and the low-lying excited states) of any d -dimensional gapped local quantum Hamiltonian displays area law scaling: $S_\ell \sim \ell^{d-1}$, where ℓ denotes the linear subsystem dimension⁵. For gapless Hamiltonians, S_ℓ receives an additional logarithmic corrections $S \sim \ell^{d-1} \ln \ell$. For $d = 1$ where these statements can be rigorously proved, $S_\ell \sim \ln \ell$ at a critical point; the coefficient of the log term is given by the central charge c of the conformal field theory which describes the critical point⁷. In contrast, ρ_{red} corresponding to mid-spectrum eigenstates of a generic Hamiltonian usually shows volume law entanglement: $S_\ell \sim \ell^d$.

The physics of closed quantum systems subjected to a periodic drive has received tremendous attention in recent past⁸⁻¹⁷. Such systems are typically described by their Floquet Hamiltonian H_F which is related to their evolution operator U by $U(T, 0) = \mathcal{T}_t \exp[-i \int_0^T dt H(t)/\hbar] = \exp[-i H_F T/\hbar]$. The interest in such systems is partly due to the presence of experimental platforms such as ultracold atoms in optical lattice where such phenomena may be experimentally tested¹⁸⁻²². Moreover these driven systems allow one to explore several phenomena such as time crystalline state of matter²³⁻²⁵, dynamical freezing²⁶⁻³⁰, dynamical localization³¹⁻³³, generation of topologically non-trivial Floquet phases³⁴⁻³⁸, dynamical transitions³⁹⁻⁴¹, prethermal Floquet realization of quantum scars⁴²⁻⁴⁴ and Hilbert space fragmentation⁴⁵; most of these phenomena have no equilibrium analogue.

More recently, there has been a lot of interest in study of non-Hermitian quantum systems⁴⁶⁻⁵⁹. This is due to the fact that such systems can now be engineered in several experimental platforms⁶⁰ and that they often serve as models for studying open quantum systems. An explicit example of the latter phenomena constitutes study of an Ising spin chain in the presence of a measuring operator which measures $\hat{n}_j = (1 + \tau_j^z)/2$ (where τ_j^z denotes the usual Pauli matrix representing the spin on site j of the chain) with a rate γ and in the so-called no-click limit^{61,62}; this leads to a complex magnetic field term $\sim \gamma$ in the effective Hamiltonian of the spin chain. Moreover, such systems often exhibit several physical properties that have no Hermitian analogue; these include presence of exceptional points in the spectrum⁶³⁻⁶⁷, realization of skin effect⁶⁸⁻⁷⁰ leading to novel bulk-boundary correspondence^{65,67}. More recently, quantum dynamics of such systems have also been studied⁷¹⁻⁷⁵. In particular, the presence of an emergent approximate symmetry in driven non-Hermitian Ising chain has been pointed out recently⁷⁶.

In this work, we study the nature of entanglement in a driven non-Hermitian Ising chain whose Hamiltonian is given by

$$H = -J \sum_j \tau_j^x \tau_{j+1}^x - (h(t) + i\gamma/2) \sum_j \tau_j^z \quad (1)$$

where $J > 0$ denotes the strength of the ferromagnetic interaction term while $h(t) + i\gamma/2$ denotes the complex transverse field. The drive is implemented by making the real part of the transverse field time dependent via a given protocol. In what follows, we shall use either the continuous drive protocol for which

$$h(t) = h_1 + h_0 \cos(\omega_D t) \quad (2)$$

or the square-pulse protocol which can be described by

$$h(t) = h_1 + (-)h_0 \quad \text{for } t > (\leq)T/2. \quad (3)$$

Here $T = 2\pi/\omega_D$ is the drive period and h_0 denotes the drive amplitude. In the rest of this work, we shall mostly be interested in the subsystem size (ℓ) dependence of the steady-state entanglement entropy S_ℓ of such driven system as a function of ω_D and γ . We note that whereas such dependence has been studied for quench protocol earlier⁷⁵; however, it has not been analyzed for periodically driven systems.

The central results that we obtain from such a study are as follows. First, in the high drive frequency and amplitude regime, we find a phase transition for entanglement at a critical γ_c . For $\gamma \leq \gamma_c$, the entanglement show a log scaling with subsystem size. In particular, we study the half-chain entanglement $S_{L/2} \equiv S_{\ell=L/2}$ which scales as $S_{L/2} \sim \ln L$ for $\gamma \leq \gamma_c$. For $\gamma > \gamma_c$, $S_{L/2}$ is constant and is independent of the subsystem size. The critical transition value γ_c depends on the drive frequency in a non-monotonic manner and vanishes at special drive frequencies $\omega_D = \omega_m^*$ where an approximate emergent symmetry controls the behavior of the driven chain⁷⁶. We note that the role of such an emergent symmetry behind entanglement transitions in these systems has not been pointed out so far in the literature.

Second, we analyze this phase diagram and provide an analytic, albeit approximate, expression of the entanglement entropy in the thermodynamic limit. Our analytical result for S , which matches quite well with exact numerics, allows us to explain the lack of volume law scaling of the entanglement which is normally expected for driven Ising chains; moreover, it provides an expression of the coefficient of the leading $\ln L$ term leading to an analytic understanding of the phase diagram in the high drive amplitude regime. Our analysis also shows that the contribution of the jump singularities⁷⁷⁻⁷⁹ in the correlation functions of the driven chain to S is key to its logarithmic dependence on ℓ ; thus it identifies the Fisher-Hartwig singularities of the correlation functions as the reason for the entanglement transitions. To the best of our knowledge, this connection was not identified in the literature before.

Third, we provide numerical study of the entanglement in the low and intermediate frequency regime. Our analysis in this regime allows us to identify a length scale $\ell^*(\omega_D)$ which diverges at low-frequency. For $\ell \leq \ell^*(\omega_D)$, the effective Floquet Hamiltonian for the subsystem behaves as an effective long-range Hamiltonian; consequently, the entanglement shows volume-law scaling in this regime for small γ : $S_\ell \sim \ell$. As ℓ increases and exceeds $\ell^*(\omega_D)$, S crosses over from linear to logarithmic scaling. For large γ , S remains independent of ℓ for all ℓ ; the transition between these two regimes occurs at a critical value of γ similar to the high drive-frequency regime.

The plan of the rest of the paper is as follows. In Sec. II we present our analytical results; in Sec. II A, we analyze the driven chain to obtain the analytic, albeit perturba-

tive, Floquet Hamiltonians for different drive protocols and identify their emergent symmetry. We also present expressions for the correlation functions and analyze their features. This is followed by Sec. II B where we present analytic computation of the half-chain entanglement entropy. Next, in Sec. III, we present our numerical result for S_ℓ ; the phase diagram in the high drive amplitude and drive frequency regime is presented in Sec. III A and compared with the analytical results obtained in Sec. II B while the low and intermediate drive frequency regimes are discussed in Sec. III B. Finally, we discuss our main results and their applicability to other integrable models and conclude in Sec. IV. Some additional details of the calculations are presented in the appendices.

II. ANALYSIS OF THE DRIVEN CHAIN

In this section, we shall provide our analytical results which turns out to be accurate in the high drive amplitude regime. The basic properties of the Floquet Hamiltonian are discussed in Sec. II A while the calculation of the entanglement entropy is charted in Sec. II B.

A. Perturbative Floquet Hamiltonian

The driven Hamiltonian of the Ising chain in the presence of complex transverse field is given by Eq. 1. The drive protocol used could either be continuous (Eq. 2) or discrete (Eq. 3). In what follows, we shall obtain analytic expression for the Floquet Hamiltonian which will be useful for computation of the correlation functions for the driven model. The analysis of this section will closely follow Ref. 76.

We begin by mapping Eq. 1 into a system of free two-components fermions; this is achieved by the well-known Jordan-Wigner transformation given by

$$\tau_j^{+(-)} = \left(\prod_{\ell=1}^{j-1} -\tau_\ell^z \right) c_j^\dagger(c_j), \quad \tau_j^z = 2c_j^\dagger c_j - 1 \quad (4)$$

where c_j denotes annihilation operator of the fermions on site j .

$$\hat{c}_j = \frac{1}{\sqrt{N}} \sum_{k \in \text{BZ}} e^{i\pi/4} e^{-ikj} \hat{c}_k \quad (5)$$

where BZ indicates the Brillouin zone $-\pi \leq k \leq \pi$. Using Eq. 4, and denoting the two component fermion field in momentum space as $\psi_k = (c_k, c_{-k}^\dagger)^T$, where c_k annihilates a fermion with momentum k , Eq. 1 can be written as

$$H = 2 \sum_{k \in \text{BZ}/2} \psi_k^\dagger H_k \psi_k$$

$$H_k = \sigma_z (h(t) - \cos k + i\gamma/2) + (\sigma_+ \sin k + \text{h.c.}) \quad (6)$$

where $\vec{\sigma} = (\sigma_x, \sigma_y, \sigma_z)$ are standard Pauli matrices in particle-hole space of the fermions, J and the lattice spacing a is set to unity, $\text{BZ}/2$ denotes positive half of the Brillouin zone, and $\sigma^\pm = \sigma_x \pm i\sigma_y$.

The first-order contribution to the Floquet Hamiltonian can be computed perturbatively using standard prescription of FPT^{17,76}. Following the derivation sketched in App. A, one obtains $H_F^{(1),c(s)} = \frac{i\hbar}{T} U_1^{c(s)}(T)$ where

$$H_F^{(1),c(s)} = \sum_k \psi_k^\dagger [S_{1k}\sigma_z + (S_{2k}\sigma^+ + \text{h.c.})] \psi_k \quad (7)$$

$$\begin{aligned} S_{1k} &= 2(\hbar_1 - \cos(k) + i\gamma/2), \\ S_{2k} &= 2f^c(T) \sin k \quad \text{cosine protocol} \\ &= 2f^s(T) \sin k e^{-ih_0T/\hbar} \quad \text{square pulse protocol} \end{aligned}$$

where $f^{c(s)}(T)$ are given by

$$\begin{aligned} f^c(T) &= J_0(4h_0/(\hbar\omega_D)), \\ f^s(T) &= \frac{\hbar}{h_0T} \sin\left(\frac{h_0T}{\hbar}\right), \end{aligned} \quad (8)$$

where J_0 denotes the zeroth order Bessel function. We note that there are special drive frequencies at which $f^{c,s} = 0$ and $[H_F^{(1)}, \sigma_z] = 0$ leading to an emergent symmetry. These frequencies are given by $\omega_D = \omega_m^{*c(s)}$ where

$$\omega_m^{*c} = \frac{4h_0}{\hbar\eta_m}, \quad \omega_m^{*s} = \frac{2h_0}{m\hbar} \quad (9)$$

where m is an integer and η_m denotes the m^{th} zero of J_0 . This symmetry is approximate since it is violated by higher-order terms of the Floquet Hamiltonian⁷⁶; nevertheless, it was shown in Ref. 76 that such an approximate symmetry leaves its imprint on the dynamics of the system. Here we shall show that such a symmetry shapes the character of entanglement transitions of the driven non-Hermitian Ising chain. We also note here that the inclusion of the second order terms in H_F do not change

its matrix structure; it modifies S_{1k} and S_{2k} as shown in App. A. In what follows, we shall use this form of H_F to compute second-order perturbative results for the correlation functions and S_ℓ .

The evolution operator $U(nT)$ for both protocols can be expressed in terms of the eigenvalues E_k^a and eigenvectors $|a; k\rangle$ (where $a = 1, 2$) of the Floquet Hamiltonian as

$$U(nT) = \prod_k \sum_{a=1,2} e^{-iE_k^a nT} |a; k\rangle \langle a; k| \quad (10)$$

Here and in the rest of this section, we shall drop the indices c, s indicating the protocol to avoid clutter. For perturbative Floquet Hamiltonian, these quantities can be analytically obtained and are given by

$$\begin{aligned} E_k^a &= (-1)^a \sqrt{S_{1k}^2 + |S_{2k}|^2} = (-1)^a (\epsilon_k + i\Gamma_k) \\ |a; k\rangle &= \begin{pmatrix} n_{zk}^a \\ n_{xk}^a + i n_{yk}^a \end{pmatrix}, \quad n_{xk}^a = \frac{\text{Re}[S_{2k}]}{\mathcal{N}_{ak}} = \frac{q_{ak}}{\mathcal{N}_{ak}} \\ n_{yk}^a &= -\frac{\text{Im}[S_{2k}]}{\mathcal{N}_{ak}} = \frac{q'_{ak}}{\mathcal{N}_{ak}} \\ n_{zk}^a &= \frac{S_{1k} + (-1)^a E_k}{\mathcal{N}_{ak}} = \frac{p_{ak}}{\mathcal{N}_{ak}}, \\ \mathcal{N}_{ak} &= \sqrt{|S_{1k} + (-1)^a E_k|^2 + |S_{2k}|^2} \end{aligned} \quad (11)$$

Note that $n_{yk}^a = 0$ for the continuous protocol for which S_{2k} is real. The exact expressions for E_k^a and $|a; k\rangle$, however, needs to be computed numerically for the continuous drive protocol. Its computation for the square-pulse protocol can be carried out analytically as shown in App. B.

The normalized wavefunction of the driven chain starting from a state $|\psi_0\rangle = \prod_k (u_{0k} + v_{0k} c_k^\dagger c_{-k}^\dagger) |0\rangle$ can be written, in terms of these Floquet eigenvalues and eigenvectors as $|\psi(nT)\rangle = \prod_k |\psi_k(nT)\rangle$ where

$$\begin{aligned} |\psi_k(nT)\rangle &= (u_k(nT) + v_k(nT) c_k^\dagger c_{-k}^\dagger) |0\rangle, \quad u_k(nT) = \frac{\sum_a e^{-iE_k^a nT} p_{ak} (u_{0k} p_{ak}^* + v_{0k} (q_{ak}^* + i q'_{ak}^*))}{\mathcal{D}_k(nT)} \\ v_k(nT) &= \frac{\sum_a e^{-iE_k^a nT} (q_{ak} - i q'_{ak}) (u_{0k} p_{ak}^* + v_{0k} (q_{ak}^* + i q'_{ak}^*))}{\mathcal{D}_k(nT)} \\ \mathcal{D}_k(nT) &= \left[\left| \sum_a e^{-iE_k^a nT} p_{ak} (u_{0k} p_{ak}^* + v_{0k} (q_{ak}^* + i q'_{ak}^*)) \right|^2 + \left| \sum_a e^{-iE_k^a nT} (q_{ak} - i q'_{ak}) (u_{0k} p_{ak}^* + v_{0k} (q_{ak}^* + i q'_{ak}^*)) \right|^2 \right]^{1/2} \end{aligned} \quad (12)$$

and $|0\rangle$ denotes the fermion vacuum.

It is well-known that the computation of entanglement entropy for integrable Ising chains begins with analysis of the correlation functions of the model. We denote these correlation functions, computed, at the end of n drive

cycles, as

$$\begin{aligned} \Pi_{xk}(nT) &= \langle \psi_k(nT) | (c_k^\dagger c_{-k}^\dagger + \text{h.c.}) | \psi_k(nT) \rangle \\ &= 2\text{Re}(u_k^*(nT) v_k(nT)) \\ \Pi_{zk}(nT) &= -i \langle \psi_k(nT) | (c_{-k} c_k - c_k^\dagger c_{-k}^\dagger) | \psi_k(nT) \rangle \\ &= 2\text{Im}(u_k^*(nT) v_k(nT)) \\ \Pi_{yk}(nT) &= \langle \psi_k(nT) | (2c_k^\dagger c_k - 1) | \psi_k(nT) \rangle \\ &= 2|v_k(nT)|^2 - 1 \end{aligned} \quad (13)$$

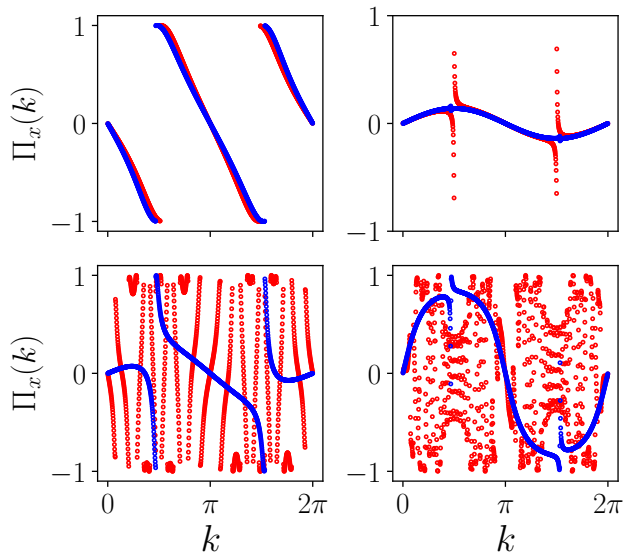


FIG. 1: Plot of Π_{xk} as a function of k for $\hbar\omega_D = 60J$ (top left panel), $\hbar\omega_D = \hbar\omega_1^* \simeq 33.26J$ (top right panel), $\hbar\omega_D = 0.7J$ (bottom left panel) and $\hbar\omega_D = 0.1J$ (bottom right panel). The red lines display results from exact numerics while the blue lines show that obtained using second order Floquet perturbation theory. For all plots $\gamma = 0.01J$, $h_0 = 20J$, $h_1 = 0.1J$ and $L = 1000$. See text for details.

The plots of the steady state correlation function $\Pi_{xk}^{\text{steady}} \equiv \Pi_{xk}$ at large drive frequencies are shown in top panels of Fig. 1 for the continuous drive protocol and $\gamma = 0.01J$. The coefficients of the steady state wavefunction $|\psi_k^{\text{steady}}\rangle$ are denoted by u_k^{steady} and v_k^{steady} and are charted out in App. B for the square pulse protocol. For the continuous protocol, the procedure is analogous; however, the exact steady state wavefunction needs to be obtained numerically. The steady state value of Π_{xk} are obtained by replacing $u_k(nT)$ and $v_k(nT)$ in Eq. 13 by u_k^{steady} and v_k^{steady} respectively. We have checked numerically that $|\psi_k(nT)\rangle$ coincides with the steady state correlation functions obtained using the above-mentioned procedure after n drive cycles, where n depends on both ω_D and γ , for both protocols. This feature has been explicitly checked for all plots presented in this work.

From Fig. 1, we find that for generic drive frequencies $\omega_D \neq \omega_m^*$, as shown in the top left panel of Fig.1, Π_{xk} shows jump singularities at $k = \pm k^* \simeq \arccos h_1$. In contrast, at the special drive frequency $\omega_D = \omega_1^*$, the jump singularity disappears and we obtain a smooth function for Π_{xk} . For $\omega_D \neq \omega_m^*$, the second order Floquet result (blue line) matches its exact numerical counterpart (red line) quite well. In contrast, at $\omega_D = \omega_m^*$ and small values of γ , one gets a qualitative match between the two results and needs to go beyond 2nd order FPT for a quantitative match. At intermediate ($\omega_D = 0.7J$) and low ($\omega_D = 0.1J$) drive frequencies, the perturbative Floquet theory clearly breaks down as can be seen from the

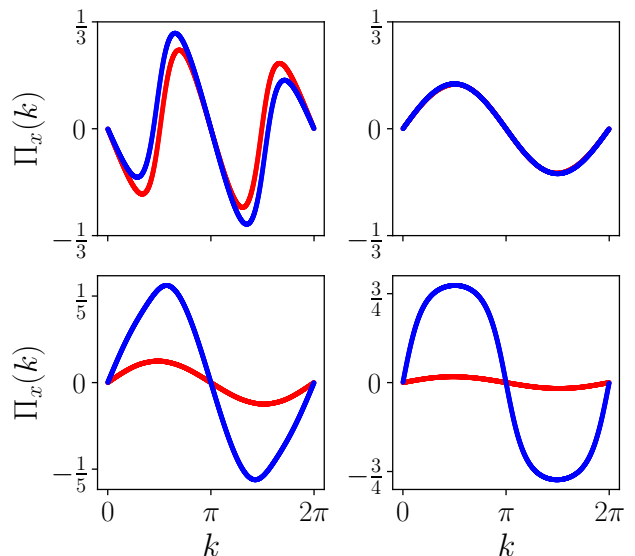


FIG. 2: Plot of Π_{xk} as a function of k for $\gamma = 2J$. All other parameters are same as in Fig. 1. See text for details.

bottom panels of Fig. 1. Here exact numerics reveals multiple jump singularities of Π_{xk} ; the number of such jump singularities increases as ω_D is lowered.

In contrast at large $\gamma \sim J$, Π_{xk} does not show any jumps singularities. As shown in Fig. 2 for $\gamma = 2J$, for all drive frequencies, Π_{xk} is a smooth function of k . The second order Floquet Hamiltonian, once again, yields a nice match with exact numerics at the high drive frequency regime.

In contrast to Π_{xk} , the functions Π_{yk} do not display any jump singularities in the high drive frequency regime and stays close to zero for $k \sim \pm k^*$. The behavior of Π_{zk} is qualitatively similar to Π_{xk} except for the fact that the magnitude of the jump singularity tends to zero at high frequencies and low γ/J where the contribution of Π_{zk} to the entanglement entropy becomes small. We shall use these features of the correlation function to compute the entanglement entropy in the next section.

B. Analytical results for the entanglement entropy

In this section, we present an analytic computation of the entanglement entropy S_ℓ for the high drive amplitude regime, where the correlation functions obtained from perturbative Floquet Hamiltonian agrees well with exact numerics. We shall carry out this calculation in the regime where the dimensionless parameter $\gamma \ll |\tilde{h}_1 f^{c(s)}(T)| \equiv |2\sqrt{1-h_1^2} f^{c(s)}(T)|$. Note that this indicates that such a computation is expected to yield more quantitatively accurate results away from the special frequencies.

To compute S_ℓ , we begin with expressions of $\hat{\Pi}_k = (\Pi_{xk}, \Pi_{yk}, \Pi_{zk})$ where $\hat{\Pi}_k$ denotes the correlator values

in the steady state. We first note that the normalization of u_k and v_k leads to conservation of the norm of the correlation functions $|\hat{\Pi}_k| = 1$. As is well-known in the literature, under such conditions, Szegő's theorem necessitates that S_ℓ can not have a term linear in ℓ . The derivation of this is sketched in App. C.

To obtain S_ℓ , we first define the correlation matrix for the system. To this end, we construct the quantity

$$\eta_k = \lambda I - \hat{\Pi}_k \quad (14)$$

which shall be central to computing S_ℓ . In what follows we shall provide an approximate analytic computation of S_ℓ in the regime where $H_F^{(1)}$ provides a reasonable description of the driven system. Following the calculations in App. A and B, in this regime, one can define the steady state wavefunctions to be

$$|\psi\rangle = \prod_{k>0} \left(u_k^{(1)} + v_k^{(1)} \hat{c}_k^\dagger \hat{c}_{-k}^\dagger |0\rangle \right)$$

$$u_k^{(1)} = \frac{n_{zk} + \text{sgn}(\Gamma_k)}{\mathcal{N}_k} \quad v_k^{(1)} = \frac{n_{xk} + in_{yk}}{\mathcal{N}_k}. \quad (15)$$

where $\mathcal{N}_k = \mathcal{N}_{\pm k}$ for $\Gamma_k > (<)0$. Substituting Eq. 15 in Eq. 13, one obtain the correlation functions $\hat{\Pi}_k^{(1)}$

$$\begin{aligned} \Pi_{xk}^{(1)} &= \frac{2 \text{Re}[(n_{zk} + \text{sgn}(\Gamma_k))^* (n_{xk} + in_{yk})]}{\mathcal{N}_k^2} \\ \Pi_{yk}^{(1)} &= \frac{2 \text{Im}[(n_{zk} + \text{sgn}(\Gamma_k))^* (n_{xk} + in_{yk})]}{\mathcal{N}_k^2} \\ \Pi_{zk}^{(1)} &= 1 - 2 \frac{|n_{zk} + \text{sgn}(\Gamma_k)|^2}{\mathcal{N}_k^2} \end{aligned} \quad (16)$$

Near the jump singularities at $k = \pm k^* = \pm \arccos(h_1)$, where Γ_k changes sign, Eq. 16 can be further simplified, for small γ , to yield

$$\begin{aligned} \Pi_{xk}^{(1)} &= \delta \text{Sgn}(\tilde{h}_1 f(T)) \frac{k - \text{Sgn}(k)k^*}{|k - \text{Sgn}(k)k^*|} \\ \Pi_{zk}^{(1)} &= \sqrt{1 - \delta^2} \text{Sgn}(k), \quad \Pi_{yk}^{(1)} = 0 \\ \delta &= \sqrt{1 - \left(\frac{\gamma}{\tilde{h}_1 f(T)} \right)^2} \end{aligned} \quad (17)$$

where we have ignored higher order terms in $k \pm k^*$. We note that for small γ and away from the special frequencies where $|\delta| \sim 1$, $\Pi_{xk}^{(1)} \gg \Pi_{zk}^{(1)}$. In this regime $\Pi_{xk}^{(1)}$ jumps around $k = \pm k^*$; these jumps control the ℓ dependence of S_ℓ , as shall be elaborated later in this section. In contrast, for large γ/J or around $\omega_D = \omega_m^*$ at which $f(T) \simeq 0$, the off-diagonal terms of the Floquet Hamiltonian will be small in the high-drive frequency regime. This leads to a steady state which closely mimics one of the eigenstates of $\hat{\tau}^z$ depending on $\text{Sgn}[\Gamma_k]$. Hence $\Pi_{zk}^{(1)}$ dominates at these frequencies and $\hat{\Pi}_k^{(1)}$ becomes a smooth function of k leading to a different behavior of S_ℓ . The transition between these behaviors which constitutes

the entanglement transition occurs around $\delta \sim 0$; thus δ controls the behavior of S_ℓ in this regime.

To obtain an analytic expression of S_ℓ for large ℓ we now carry out a Fisher-Hartwig analysis⁷⁷⁻⁷⁹. We note that this analysis can be done only when the correlation matrix depends on a single Pauli matrix. The reason for this has been discussed extensively in the literature^{78,79} and stems from the fact that such an analysis requires the correlation matrix of the model to be in the standard Toeplitz form⁷⁷; for $\hat{\Pi}_k$ with multiple components leading to block-Toeplitz form of the correlation matrix such an analysis does not hold^{78,79}. We shall therefore focus on the regime $\delta \sim 1$ where $\hat{\Pi}_k \simeq (\Pi_{xk}, 0, 0)$ and focus on the form of Π_{xk} near $k = \pm k^*$ given by Eq. 17. In this case, one can define

$$\zeta_k = \lambda - \Pi_{xk} \quad (18)$$

which acts as generators for the elements of the correlation matrix.

Next, we cast ζ_k in a form which is convenient for analysis of contribution of the singularities. To this end, we note that the form of Π_{xk} given in Eq. 17 holds only near the jump singularities at $k = \pm k^*$; the functional dependence of Π_{xk} over the entire Brillouin zone $-\pi \leq k \leq \pi$ is not captured by Eq. 17. It is well-known that the precise nature of this functional form is not important for computing the contribution of the singularities to S_ℓ ⁷⁷. Thus one can replace Π_{xk} away from the singularities by an appropriate form which allows for further analytical progress. The simplest such form will be to replace $\Pi_{xk} = \delta$ everywhere away from the singularities at $k = \pm k^*$. However since the jumps for $k = k^*$ and $k = -k^*$ occur in opposite direction as one traverse from $k = -\pi$ to $k = \pi$, one can not replace Π_{xk} by a constant without introducing intermediate spurious singularities, say, at $k = 0$ and $k = \pi$. Keeping this in mind, we use the form

$$\begin{aligned} \Pi_{xk}^{(1)} &= \text{Sgn}(\tilde{h}_1 f(T)) \text{Sgn}(k - k^*), \quad 0 < k < \pi \\ &= \text{Sgn}(\tilde{h}_1 f(T)) \text{Sgn}(k + k^*), \quad -\pi < k < 0 \end{aligned} \quad (19)$$

We shall use this form to compute S_ℓ analytically; the additional contribution due to the spurious singularities shall be subtracted out at the end of the calculation.

Using Eqs. 18 and 19, one can compute the eigenvalues of the correlation matrix in the steady state

$$\begin{aligned} \mathcal{D}_\ell(\lambda) &= \lambda I - B_\ell \otimes \sigma_x, \\ B_\ell &= \begin{pmatrix} \Pi_0 & \Pi_{-1} & \dots & \Pi_{1-\ell} \\ \Pi_1 & \Pi_0 & \dots & \Pi_{2-\ell} \\ \dots & \dots & \dots & \dots \\ \Pi_{\ell-1} & \Pi_{\ell-2} & \dots & \Pi_0 \end{pmatrix}, \\ \Pi_\ell &= \frac{1}{2\pi} \int_0^{2\pi} dk e^{i\ell k} \Pi_{xk}^{(1)} \end{aligned} \quad (20)$$

This calculation, which constitutes standard steps in Fisher-Hartwig analysis⁷⁷⁻⁷⁹ is charted out in App. D

and yields

$$\ln(\text{Det}(\mathcal{D}_\ell(\lambda))) = 2[\ell \ln(F[\eta(\lambda)]) - \sum_{i=1,3} \beta_i^2(\lambda) \ln(\ell)] + \dots$$

$$F[\eta(\lambda)] = \sqrt{\lambda^2 - \delta^2}$$

$$\beta_1 = \beta_3 = \frac{1}{2\pi i} \ln\left(\frac{\lambda - \delta}{\lambda + \delta}\right) \quad (21)$$

where the ellipsis represent subleading terms which we shall ignore for the rest of the analysis, we have subtracted out the contributions from the spurious singularities at $k = 0, \pi$, and $\beta_{1,3}$ depicts the contribution of the jump singularities at $\pm k^*$ to $\text{Det}(\mathcal{D}_\ell)$. Note that the first term in Eq. 21 constitutes contribution from the non-singular part of η_k as shown in App. D. The contribution of such term to S_ℓ vanishes as shown in App. C for $\delta = 1$. In the rest of this section, we shall estimate the contribution of the second term which yields the $\ln \ell$ behavior.

The contribution of the second term in the expression of $\ln \mathcal{D}_\ell$ to S_ℓ can be computed by defining the function $e(x, \lambda)$

$$e(x, \lambda) \equiv -\frac{x + \lambda}{2} \ln \frac{x + \lambda}{2} - \frac{x - \lambda}{2} \ln \frac{x - \lambda}{2} \quad (22)$$

The entanglement entropy can be written in the form $S_\ell = \sum_{m=-\ell}^{\ell} e(\delta, \nu_m)$ where ν_m denote the eigenvalues of the correlation matrix B_ℓ which lie within the range $-\delta \leq \nu_m \leq \delta$ with the property $\nu_m = -\nu_{-m}$. To connect S_ℓ to \mathcal{D}_ℓ , we note, from Eq. 20, that $\mathcal{D}_\ell(\Lambda) = \prod_{m=-\ell}^{\ell} (\lambda - \nu_m)$. Thus one can write

$$S_\ell = \frac{1}{4\pi i} \oint d\lambda e(\delta, \lambda) \frac{d}{d\lambda} \ln(\text{Det}(\mathcal{D}_\ell(\lambda))) \quad (23)$$

where the contour encircles the zeroes of $\text{Det}(\mathcal{D}_\ell(\Lambda))$. We now substitute Eq. 21 in Eq. 23 to evaluate S_ℓ and concentrate on the coefficient of $\ln \ell$ in the limit of small δ . A straightforward calculation yields

$$S_\ell = \delta I_1 \ln \ell + \mathcal{O}(\delta - 1) \quad (24)$$

$$I_1 = \frac{2}{\pi^2} \oint d\lambda e(1, \lambda) \frac{\beta_1(\lambda)}{\lambda^2 - 1} = \frac{2}{\pi^2} \int_0^1 dx \frac{\ln(1-x)}{x} = \frac{1}{3}$$

For $\delta = 1$ which is achieved in the quench limit when $T, \gamma \rightarrow 0$, we obtain $S_\ell = 1/3 \ln \ell$ which reproduces the result obtained in Ref. 75 as a special case. For the driven system, δ is a non-monotonic function of the drive frequency whose precise form depends on the drive protocol through $f(T)$. This allows us to infer that $S_\ell(T)$ will be a non-monotonic function of T . We shall compare this analytic form of S_ℓ with exact numerical results at small γ and high drive frequency regime in the next section.

Before ending this section, we would like to discuss two salient points of our analysis. First, the approximating $\hat{\Pi}_k$ with only one of its components, namely Π_{xk} , violates the normalization of $\hat{\Pi}(k)$ for all $\delta(T) \neq 1$. This in turn leads to a spurious volume law term; this term

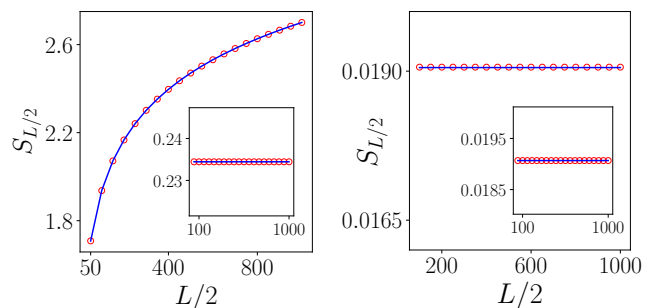


FIG. 3: Left Panel: Plot of steady-state half-chain entanglement $S_{L/2}$ as a function of L showing logarithmic dependence of $S_{L/2}$ at small $\gamma = 0.1J$ and $\hbar\omega_D/J = 60$: $S_{L/2} \sim \alpha \ln L + \text{constant}$. A fit of $S_{L/2}$ estimates $\alpha \sim 0.3314$ which is close to its analytically predicted value $1/3$. The inset shows $S_{L/2}$ at $\gamma = 2J$ indicating its independence on L : $S_{L/2} = \text{constant}$. Right Panel: Same as in left panel but at $\omega_D = \omega_1^{*c}$ where $S_{L/2}$ is independent of L for both small ($\gamma = 0.1J$) and large ($\gamma = J$) γ . For all plots, the red dots indicate numerical data and blue lines represent the fit, $h_0 = 20J$, $h_1 = 0.1J$. See text for details.

can be obtained when the first term of $\ln \mathcal{D}_\ell(\lambda)$ (which is $\sim \ell$) in Eq. 21 is substituted in Eq. 23. Second, the $\mathcal{O}(\delta - 1)$ terms in Eq. 24 can not be reliably computed within this approach; it leads to a logarithmic divergence for $\delta \neq 1$. Both these features are artifacts of violation of the normalization condition of $\hat{\Pi}_k$. A more rigorous calculation keeping the full matrix structure of $\hat{\Pi}_k$ which requires the use of Fredholm techniques may resolve these issues; however, such a technique, used for computing S_ℓ for ground state of the Hermitian XY model⁷⁹, can not be straightforwardly applied in the present case due to presence of a non-zero Γ_k . We leave this issue as subject of future work.

III. NUMERICAL RESULTS

In this section, we present our numerical results on steady state entanglement entropy S_ℓ . The numerical procedure for computing $S_\ell(nT)$ for the driven state is as follows. First, for the continuous protocol, we carry out Trotter decomposition of the evolution operator $U_k(T, 0)$ and write

$$U_k(T, 0) = \prod_{j=1}^N U_k(t_j, t_{j-1}) = \prod_{j=1}^N e^{-iH(t_j)\Delta t/\hbar} \quad (25)$$

where the interval $\Delta t = t_j - t_{j-1} = T/N$; it is chosen to be small enough so that $H(t)$ does not change significantly within this interval. For the square pulse protocol, $U_k(T, 0)$ can be exactly obtained as shown in App. B. For either case, diagonalization of $U_k(T)$ leads to its eigenvalues $e^{\pm iE_k^F T/\hbar}$, where E_k^F are the exact Floquet eigenvalues, and the corresponding eigenfunctions are $|\pm; k\rangle$.

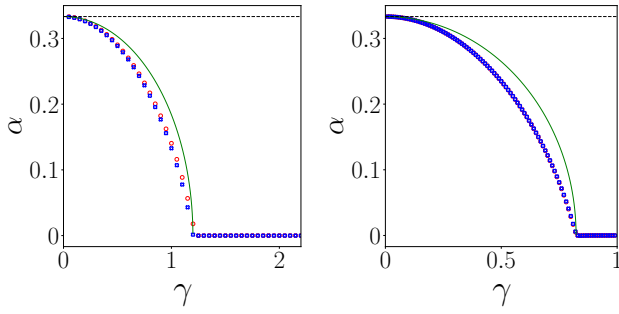


FIG. 4: Left Panel: Plot of α as a function of γ for $\hbar\omega_D/J = 60$ using continuous drive protocol, showing its decrease from $1/3$ to 0 at the critical $\gamma = \gamma_c \sim 1J$ where the entanglement transition takes place. The red and the blue dots correspond to exact numerical results and results from second order FPT respectively; the green line shows analytical result for α obtained in Eq. 24. Right panel: Same as left panel using square pulse drive protocol. The red and the blue dots correspond to exact numerical results and results from first order FPT respectively while the green line shows analytical result for α obtained in Eq. 24. The dashed line in both figures indicate $\alpha = 1/3$ and is a guide to the eye. For all plots $h_0 = 20J$, $h_1 = 0.1J$ and $L \leq 2000$.

This allows one to write

$$\begin{aligned}
 U_k(T, 0) &= \sum_{a=\pm} e^{-iaE_k^F T/\hbar} |a; k\rangle \\
 |\psi_k(nT)\rangle &= \frac{|\tilde{\psi}_k(nT)\rangle}{|\langle \tilde{\psi}_k(nT) | \tilde{\psi}_k(nT) \rangle|}, \\
 |\tilde{\psi}_k(nT)\rangle &= U_k(nT, 0) |\psi_{0k}\rangle
 \end{aligned} \tag{26}$$

Note that for non-Hermitian systems the non-conservation of norm during evolution necessitates normalization of the wavefunction at all stroboscopic times nT . Having obtained $|\psi_k(nT)\rangle$, we use it to construct the correlation functions $\Pi_k(nT)$ using Eq. 13 and follow standard procedure charted out earlier to obtain $S_\ell(nT)$. At large n , $S_\ell(nT)$ reaches its steady state value S_ℓ which we analyze below in details.

The results obtained using the above procedure for high drive amplitude and frequency region are presented and compared with their analytical counterparts (computed using perturbative Floquet Hamiltonian obtained in Sec. IIB and Apps. A and B) in Sec. IIIA. This is followed by Sec. IIIB where we present our results for the low and intermediate drive frequency regime. Most of our numerical results shall be carried out using continuous drive protocol; however, we shall also present the phase diagram corresponding to the square-pulse protocol.

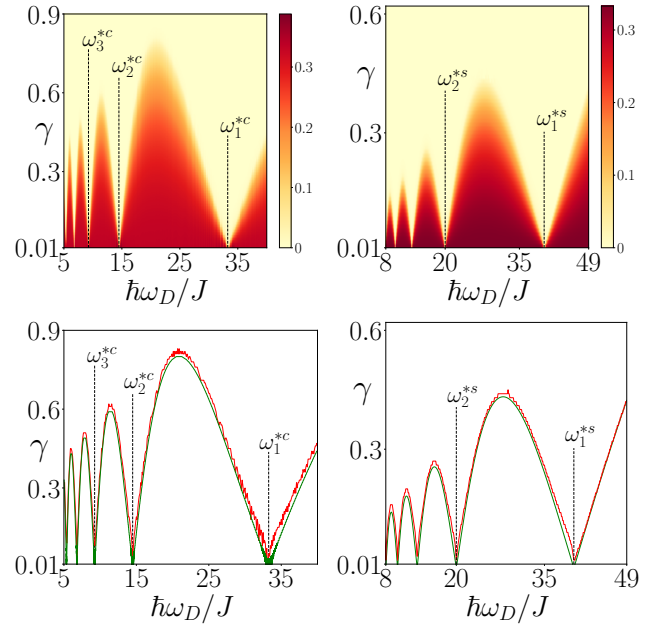


FIG. 5: Top left Panel: Plot of α , obtained from exact numerics, as a function of ω_D and γ showing the non-monotonic nature of γ_c and the positions of the special frequencies ω_m^{*c} for continuous wave drive protocol. Top right Panel: Same as top left panel obtained using square pulse drive protocol. Bottom left panel: This figure shows the phase boundary ($\alpha < 0.001$) obtained using exact numerics (red line) and analytical result (green line which corresponds to $\delta = 0$) for continuous wave drive. Bottom right panel: Same as bottom left panel obtained for square pulse drive protocol with $\alpha < 0.01$. For all plots $h_0 = 20J$, $h_1 = 0.1J$ and $L \leq 1000$. See text for details.

A. Phase diagram in the high drive amplitude regime

In the high drive amplitude and frequency regime and away from the special frequencies ω_m^* , the half-chain entanglement entropy $S_{\ell=L/2} \equiv S_{L/2}$ shows two distinct behaviors as shown in the left panel Fig. 3 as a function of L for the continuous protocol. For low $\gamma \simeq 0.1$, $S_{L/2} \simeq \alpha \ln L$; the coefficient $\alpha \sim 1/3$ in the regime of high frequency. We note that this result coincides with the behavior of S_ℓ (Eq. 24) computed in Sec IIB in the high-frequency and low γ regime where $\delta \rightarrow 1$. In contrast, for $\gamma = 2$, $S_{L/2}$ displays area law (inset of left panel of Fig. 3) and is thus independent of L . We note that this behavior is qualitatively different from that of $S_{L/2}$ at $\omega_D = \omega_1^{*c}$, where it shows area law behavior for almost all γ as shown in the right panel of Fig. 3.

For $\omega_D \neq \omega_m^*$, a transition between these two behaviors occur at a critical γ_c , as shown in the left panel of Fig. 4, where α is plotted as a function of γ . The analytic expression of S_ℓ predicts $\alpha = \delta/3$ leading to vanishing of α at $\gamma^* \simeq |\hbar_1 f(T)|$ ($\delta = 0$). This prediction seems to match the numerical result qualitatively as also shown in

the left panel of Fig. 4. The right panel of Fig.4 shows similar results for the square pulse drive protocol. Note that we do not expect a quantitative agreement here since the analytic computation of S_ℓ is expected to be accurate only for $\delta \sim 1$.

The phase diagram demonstrating this entanglement transition as a function of the drive frequency ω_D and the measurement rate γ is given in Fig.5. The top left panel of Fig. 5 plots α as a function of γ and ω obtained from fitting the data for $L \leq 1000$; this data is obtained using trotter decomposition of the evolution operator for the continuous drive protocol. The region where $\alpha \simeq 0$ marks the boundary for entanglement transition as shown in the bottom left panel of Fig. 5. The numerical cutoff for obtaining this boundary is set to be $\alpha < 0.001$. A similar phase diagram and boundary for the square pulse drive protocol is shown in the right panels of Fig. 5. The red lines in the bottom panels indicate the numerical phase boundaries. The plots clearly demonstrate the non-monotonic dependence of the phase boundary of the entanglement transition on the drive frequency. The green lines in the bottom panels of Fig. 5 indicate the curves $\delta = 0$ for the continuous (bottom left) and the square pulse (bottom right) drive protocols. It is evident that in this regime the analytical result matches exact numerics quite well.

This behavior of S_ℓ can also be qualitatively understood from the first order Floquet Hamiltonian as follows. The energy eigenvalues corresponding to the first order Floquet Hamiltonian (Eq. 7) is given by $E_k^\pm = \pm E_k = \pm 2\sqrt{(h_1 - \cos k + i\gamma/2)^2 + (f^{(c,s)}(T) \sin k)^2}$. For small γ and $f^{(c,s)}(T) \neq 0$, $\gamma^2 < 4[(h_1 - \cos k)^2 + (f^{(c,s)}(T) \sin k)^2]$ and one has $\Gamma_k = \text{Im}[E_k] \sim \gamma(h_1 - \cos k)$. Thus Γ_k changes sign around $k^* \simeq \arccos(h_1)$ leading to jumps in $\text{Sgn}[\Gamma_k]$, while $\epsilon_k = \text{Re}[E_k]$ varies smoothly having the same signature over the full BZ. This gives rise to jumps in $\Pi_x(k)$, as can be seen from top left panel of Fig. 1.

In contrast for $\gamma^2 \gg 4[(h_1 - \cos k)^2 + (f^{(c,s)}(T) \sin k)^2]$, one has $\Gamma_k \sim \gamma$. In this regime, Γ_k does not change sign, while ϵ_k smoothly changes sign across $k \sim \pm k^*$. Hence no jumps occur in $\Pi_x(k)$ for any k as can be seen from the top left panel of Fig. 2. Since the coefficient α of the $\ln \ell$ term in S_ℓ receives contribution from the jump singularities in the correlation function, it vanishes for large γ leading to area law behavior. In contrast for small γ , the jumps persist and α remain finite leading to a finite $\ln \ell$ term in S_ℓ . This allows one to expect two different phases separated by a transition at $\gamma = \gamma_c$ for which $\alpha(\gamma_c) = 0$. We also note when $f^{(c,s)}(T)$ vanish $\Gamma_k \sim \gamma$ for almost all γ while ϵ_k smoothly changes sign across $k \sim \pm k^*$. The correlation functions therefore remain smooth for any γ . This leads to an area-law behavior for almost all γ and $\gamma_c \rightarrow 0$.

Thus we find that in the high drive amplitude and frequency regime it is possible to traverse between different phases (for which $S_\ell \sim \ln \ell$ and $S_\ell \sim \text{constant}$) through the entanglement transition by tuning the drive

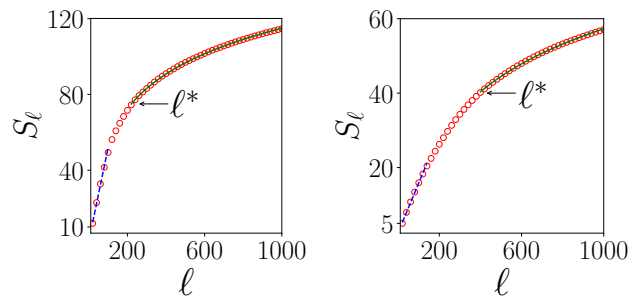


FIG. 6: Left Panel: Plot of S_ℓ as a function of ℓ for $\gamma = 0.001J$ and $\hbar\omega_D/J = 0.1$ showing linear behavior at small ℓ for the continuous drive protocol. Right panel: Similar plot for $\hbar\omega_D/J = 0.01$ showing qualitatively similar behavior. The plots indicate a subsequent crossover to $\ln \ell$ behavior beyond a crossover scale ℓ^* indicated by the arrows. Note that ℓ^* increases with decreasing drive frequency. For all plots $h_0 = 20J$, $h_1 = 0.1J$. See text for details.

frequency. In addition, the approximate emergent symmetry at special drive frequencies at ω_m^* shapes the nature of these transition; near these frequencies, $\gamma^* \rightarrow 0$ and the phase featuring area law behavior of S_ℓ dominates. These features distinguish the behavior of S_ℓ in periodically driven systems from their quench counterparts studied in Ref. 75.

B. Low and intermediate drive frequencies

At low and intermediate drive frequencies, the results obtained from the perturbative Floquet Hamiltonian does not agree with those obtained from exact numerics. This is pointed out in App. B for the square pulse protocol where the exact Floquet Hamiltonian can be computed analytically. For the continuous protocol, the exact Floquet Hamiltonian can be computed numerically and it shows a similar deviation. In both cases, this feature is reflected from the bottom panels of Figs. 1 and 2 where the behavior of Π_{xk} computed using exact numerics deviates drastically from that computed using $H_F^{(2)}$.

A numerical computation of S_ℓ in the low and intermediate drive frequency regime shows two distinct regimes as shown in Fig. 6 for $\hbar\omega_D/J = 0.1$ (left panel) and $\hbar\omega_D/J = 0.01$ (right panel) for $\gamma = 0.001J$. For both of these drive frequencies, $S_\ell \sim \ell$ for $\ell \leq \ell^*$; in contrast, for $\ell > \ell^*$, we find $S_\ell \sim \ln \ell$. We note that the emergence of such a volume law for S_ℓ does not contradict Szegő's theorem which is valid for asymptotically large ℓ . Below, we investigate the origin of the crossover length scale ℓ^* in the low and intermediate drive frequency regime.

To this end, we first note that in the low-frequency regime, the steady state corresponds to an eigenstate of the Floquet Hamiltonian which corresponds to $\Gamma_k > 0$ for each k . This situation is to be contrasted with Hermitian

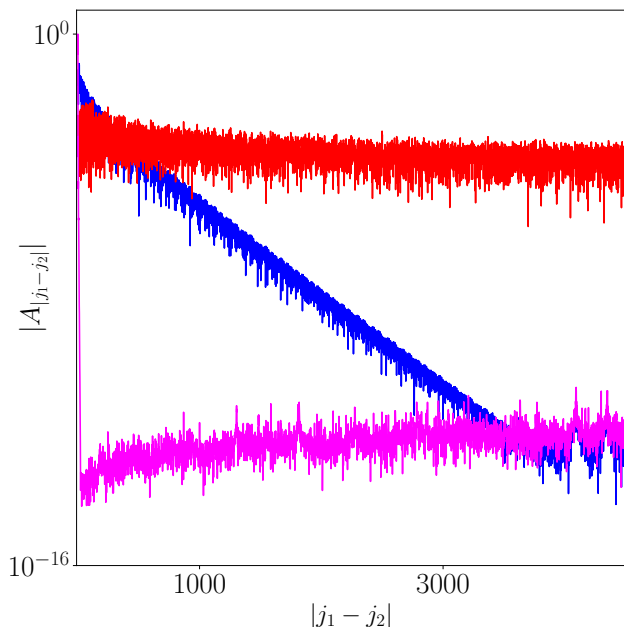


FIG. 7: Plot of A_j as a function of j for $\hbar\omega_D/J = 9$ (magenta curve), 1 (blue curve) and 0.1 (red curve) for the square pulse protocol. For all plots $h_0 = 20J$, $h_1 = 0.1J$, $\gamma = 0.001J$, and $L = 10000$. See text for details.

Ising model where it can be a superposition of both Floquet eigenvalues at every k^{40} . Thus it turns out that if the Floquet Hamiltonian develops long correlation length in real space in a drive frequency regime, one would naturally expect a volume-law entanglement for the steady state when subsystem size is smaller than the correlation length; in this regime, the effective Hamiltonian describing the subsystem becomes long-ranged⁴⁰. To check if this is indeed the case here, we resort to the square pulse protocol. Using Eqs. B2, B3, and B4, we can express the Floquet Hamiltonian in real space (up to an additive constant)

$$\begin{aligned}
 H'_F &= \sum_{j_1, j_2} \left(c_{j_1}^\dagger A_{j_1-j_2} c_{j_2} + c_{j_1} B_{j_1-j_2} c_{j_2} + \text{h.c.} \right) \\
 A_{j_1-j_2} &= \int_{-\pi}^{\pi} \frac{dk}{2\pi} e^{-ik(j_1-j_2)} \hbar \alpha_k n_{zk} \\
 B_{j_1-j_2} &= \int_{-\pi}^{\pi} \frac{dk}{2\pi} e^{i\pi/2} e^{-ik(j_1-j_2)} \hbar \alpha_k (n_{xk} - i n_{yk}) \quad (27)
 \end{aligned}$$

For the continuous protocol, an analogous expression for $A_{j_1-j_2}$ and $B_{j_1-j_2}$ exists; however α_k and \vec{n}_k need to be obtained numerically. Below we discuss numerical computation of $A_{j_1-j_2}$; the results obtained for $B_{j_1-j_2}$ are similar and shall not be discussed separately.

A numerical computation of $A_{j_1-j_2}$ indicates $|A_{j_1-j_2}| \sim \exp[-|j_1 - j_2 - 1|/\ell^*(\omega_D)]$ as shown in Fig. 7 for the square-pulse drive protocol with $\gamma = 0.001J$ and $\hbar\omega_D/J = 9, 1.0$ and 0.1 . The length scale ℓ^* , which controls the effective short- or long-range

nature of the Floquet Hamiltonian, can be obtained by standard fitting procedure.

As can be clearly seen from Fig. 7, ℓ^* increases with decreasing drive frequency. At high and intermediate drive frequencies, $\ell^*(\omega_D) \rightarrow 0$ (magenta curve in Fig. 7) signifying that the Floquet Hamiltonian is well described by a nearest-neighbor fermion hopping model. With decreasing ω_D , ℓ^* increases; this indicates when the subsystem size $\ell < \ell^*$, S_ℓ in the steady state mimics features of a long-range model. This leads to a volume-law behavior. In contrast, for $\ell \geq \ell^*(\omega_D)$, the entanglement is still due to an effectively short-range model and we get the expected logarithmic behavior. The crossover between these two regimes occur around $\ell = \ell^*(\omega_D)$ as can be seen from Fig. 6.

For large γ , ℓ^* always remain small. This can be qualitatively understood from the fact that for $\gamma \gg 1$, $\alpha_k n_{zk} \sim \gamma + O(1)$ and $\alpha_k n_{xk} \sim O(1)$ and $\alpha_k n_{yk} \sim O(1)$. This indicates $\ell^* \rightarrow 0$ even in the low-drive frequency limit and one obtains area law behavior of S_ℓ for all ℓ .

IV. DISCUSSION

In this work, we have studied entanglement transitions in a periodically driven integrable non-Hermitian Ising model. The non-hermiticity of the model arises from the presence of a complex transverse field; such a non-hermitian model can originate from an Ising chain subjected to measurements in the so-called no-click limit^{61,75}. Our analysis is based on a Jordan-Wigner transformation which maps such a driven chain to a system of spinless fermions; this allows to conclude that such a study is applicable to several other spin systems such as the non-Hermitian XY model and the Kitaev chain which can be reduced to the same free fermion form by a Jordan-Wigner transformation⁷⁶.

Our analysis presents a detailed phase diagram for entanglement transition in such driven system. For high drive frequency regime, we find two phases. In the first phase which occurs when the imaginary part of the transverse field, γ , is small, the steady state entanglement shows a logarithmic dependence on the sub-system size. We provide an explicit analytic expression for the coefficient of the $\ln \ell$ term, α , in the small γ limit and show that it can be tuned using drive frequency. In particular, we find that $\alpha \rightarrow 0$ for almost all γ at some special drive frequencies; this is a consequence of an approximate emergent symmetry of the driven model. In contrast, for large γ , the entanglement exhibits an area-law behavior. We chart out the phase boundary between these phases as a function of γ and ω_D . Our analytic results based on contribution of the Fisher-Hartwig singularities to S_ℓ indicate $\alpha = \delta/3$. This result matches exact numerics in the high frequency regime quite well and shows that the entanglement transition boundary is well-approximated by the relation $\delta = 0$. We note that the tuning of α using the drive frequency and the presence of special fre-

quencies where $\alpha \rightarrow 0$ due to an approximate emergent symmetry has not been presented earlier.

We also numerically study the entanglement of the driven system at low and intermediate drive frequencies where analytic results are difficult to obtain. In this regime, we identify a length scale $\ell^*(\omega_D)$ which can be identified as the correlation length of the driven Ising chain. For subsystem size $\ell \leq \ell^*$, the driven chain sees an effective long-range Floquet Hamiltonian for small γ . Consequently, it exhibits volume law entanglement. As one increase ℓ , S_ℓ crosses over to a $\ln \ell$ behavior when $\ell > \ell^*$. The value of ℓ^* increase with decreasing ω_D . In contrast, for large γ , the driven chain always has short range correlation in the steady state; consequently, S_ℓ always exhibits area-law. We note that the emergence of such a length scale for driven non-hermitian chains has not been pointed out in the literature before.

There are several possible extensions to our work. The first of these constitutes an exact calculation of S_ℓ using Fredholm techniques for non-hermitian Ising systems; such a calculation would be an interesting application of the technique in the domain of non-hermitian quantum systems. The second is the possibility to study the entanglement of such a system away from the no-click limit; this requires analysis of the Ising chain coupled to the detector in its full generality. It will be useful to check if the entanglement transition survives in this case; this question is of relevance to possible experiments and is of particular importance in the low ω_D and low γ limit where the system takes a long time to reach the steady state. We leave these issues for future work.

In conclusion, we have studied entanglement transition in a driven non-Hermitian Ising chain and charted out the corresponding phase boundary. We have provided analytical results for S_ℓ in the high drive frequency regime and discussed its relation to an emergent approximate symmetry of the driven chain. In the low and intermediate drive frequency regime, we have identified a correlation length scale which shapes the behavior of the entanglement at low γ . We expect our results to be applicable to other, similar, non-hermitian integrable models such as the XY and Kitaev chains.

V. ACKNOWLEDGEMENT

The authors thank M. Schiro, A. Silva and J. De Nardis for discussions. KS thanks DST, India for support through SERB project JCB/2021/000030.

Appendix A: Floquet Hamiltonian

In this appendix, we sketch the derivation of the Floquet Hamiltonian starting from Eq. 6 of the main text. We first concentrate on the high drive amplitude regime where $h_0 \gg h_1, J, \gamma$. In this regime one can write

$H = H_0(t) + H_1$ where

$$\begin{aligned} H_0(t) &= \sum_k \psi_k^\dagger 2h_0(t) \sigma_z \psi_k \\ H_1 &= 2 \sum_k \psi_k^\dagger [(h_1 - \cos k + i\gamma/2) \sigma_z \\ &\quad + (\sigma_+ \sin k + \text{h.c.})] \psi_k \end{aligned} \quad (\text{A1})$$

We note that $h_0(t)$ depends on the protocol used and can be read off from Eqs. 2 and 3 for continuous and discrete drive protocols respectively.

To obtain the Floquet Hamiltonian from Eq. A1, we first construct the evolution operator corresponding to $H_0(t)$: $U_0(t, 0) \equiv U_0(t) = \exp[-i \int_0^t H_0(t') dt' / \hbar]$. A straightforward evaluation leads to⁷⁶

$$U_0^c(t) = \prod_k e^{-2ih_0 \sin(\omega_D t) \psi_k^\dagger \sigma_z \psi_k / (\hbar \omega_D)} \quad (\text{A2})$$

for the continuous protocol and

$$\begin{aligned} U_0^s(t) &= \prod_k e^{2ih_0 t \psi_k^\dagger \sigma_z \psi_k / \hbar} \quad t \leq T/2, \\ &= \prod_k e^{2ih_0(T-t) \psi_k^\dagger \sigma_z \psi_k / \hbar} \quad t > T/2. \end{aligned} \quad (\text{A3})$$

for the square pulse drive protocol. Note that $U_0(T) = I$ for both continuous and square-pulse protocols which indicates that $H_F^{(0)} = 0$.

The first-order contribution to the Floquet Hamiltonian can be computed perturbatively using standard prescription of FPT^{17,76}. One obtains

$$U_1^{c(s)}(T) = \frac{-i}{\hbar} \int_0^T dt [U_0^{c(s)}(t)]^\dagger H_1 U_0^{c(s)}(t) \quad (\text{A4})$$

This can be evaluated in a straightforward manner following Ref. 76 and leads to

$$\begin{aligned} H_F^{(1),c(s)} &= i\hbar U_1^{c(s)}(T)/T \\ &= \sum_k \psi_k^\dagger [S_{1k} \sigma_z + (S_{2k} \sigma^+ + \text{h.c.})] \psi_k \\ S_{1k} &= 2(h_1 - \cos(k) + i\gamma/2), \\ S_{2k} &= 2f^c(T) \sin k, \quad \text{cosine protocol} \\ &= 2f^s(T) \sin k e^{-ih_0 T / \hbar}, \quad \text{square pulse protocol} \end{aligned} \quad (\text{A5})$$

where

$$\begin{aligned} f^c(T) &= J_0 (4h_0 / (\hbar \omega_D)) \\ f^s(T) &= \frac{\hbar \sin(h_0 T / \hbar)}{h_0 T} \end{aligned} \quad (\text{A6})$$

The higher order corrections to the Floquet Hamiltonian has been computed in Ref. 76. These terms in p^{th} order of perturbation theory, are typically suppressed by a $1/\omega_D^{p-1}$ factor compared to $H_F^{(1)}$. For $p = 2$, such terms merely change the form of S_{1k} and S_{2k} ; they do not alter the

structure of H_F . An explicit computation carried out in Ref. 76 shows that

$$S_{1k} = (\alpha_{1k} + i\gamma) \quad S_{2k} = \Delta_k(\alpha_{2k} + i\gamma\lambda) \quad (\text{A7})$$

where $\alpha_k = 2(h_1 - \cos k)$, $\Delta_k = 2 \sin k$ and

$$\begin{aligned} \alpha_{1k} &= \alpha_k - 2\Delta_k^2 \sum_{n=0}^{\infty} \frac{J_0\left(\frac{4h_0}{\hbar\omega_D}\right) J_{2n+1}\left(\frac{4h_0}{\hbar\omega_D}\right)}{(n+1/2)\hbar\omega_D} \\ \alpha_{2k} &= J_0\left(\frac{4h_0}{\hbar\omega_D}\right) + \alpha_k\lambda \\ \lambda &= 2 \sum_{n=0}^{\infty} \frac{J_{2n+1}\left(\frac{4h_0}{\hbar\omega_D}\right)}{(n+1/2)\hbar\omega_D} \end{aligned} \quad (\text{A8})$$

These expressions for S_{1k} and S_{2k} are used for computing second-order perturbative results for the correlation matrix in the main text.

Appendix B: Exact H_F for the square pulse protocol

The evolution operator for the square-pulse drive protocol given by Eq. 3 of the main text is

$$\begin{aligned} U_k &= \prod_k e^{-iH_k^+ T/(2\hbar)} e^{-iH_k^- T/(2\hbar)} = \prod_k e^{-iH_{Fk} T/\hbar} \\ H_k^\pm &= \theta_k^\pm (r_{zk}^\pm \tau_z + r_{xk}^\pm \tau_x) \end{aligned} \quad (\text{B1})$$

$$\begin{aligned} n_{zk} \sin(\alpha_k T) &= r_{zk}^- \cos(\theta_k^+ T/(2\hbar)) \sin(\theta_k^- T/(2\hbar)) + r_{zk}^+ \cos(\theta_k^- T/(2\hbar)) \sin(\theta_k^+ T/(2\hbar)) \\ n_{yk} \sin(\alpha_k T) &= \sin(\theta_k^- T/(2\hbar)) \sin(\theta_k^+ T/(2\hbar)) (r_{xk}^- r_{zk}^+ - r_{zk}^- r_{xk}^+) \\ n_{xk} \sin(\alpha_k T) &= \cos(\theta_k^+ T/(2\hbar)) \sin(\theta_k^- T/(2\hbar)) r_{xk}^- + \cos(\theta_k^- T/(2\hbar)) \sin(\theta_k^+ T/(2\hbar)) r_{xk}^+ \\ \cos(\alpha_k T) &= \cos(\theta_k^- T/(2\hbar)) \cos(\theta_k^+ T/(2\hbar)) - (r_{zk}^- r_{zk}^+ + r_{xk}^- r_{xk}^+) \sin(\theta_k^- T/(2\hbar)) \sin(\theta_k^+ T/(2\hbar)) \end{aligned} \quad (\text{B3})$$

A few lines of straightforward manipulations show that the Floquet Hamiltonian can be expressed in terms of these unit vectors and α_k as

$$H_{Fk} = \hbar\alpha_k \vec{n}_k \cdot \vec{\sigma} \quad (\text{B4})$$

In the large drive amplitude regime where $h_0 \gg h_1, J$, $n_{yk} \rightarrow 2 \sin k (1 - \cos(2h_0 T/\hbar))/(2h_0 T \alpha_k)$, $n_{zk} \rightarrow 2(h_1 - \cos k + i\gamma/2)/(\alpha_k \hbar)$ and $n_{xk} \rightarrow 2 \sin k \sin(2h_0 T/\hbar)/(2h_0 T \alpha_k)$. Thus we recover Eq. 7 of the main text.

The Floquet eigenvalues and eigenvectors can be obtained from Eq. B4 via solution of $H_{Fk} \Psi_k^\pm = E_k^\pm \Psi_k^\pm$.

where

$$\begin{aligned} \theta_k^\pm &= 2\sqrt{(h_1 \pm h_0 + i\gamma/2 - \cos k)^2 + \sin^2 k} \\ r_{zk}^\pm &= \frac{2(h_1 \pm h_0 + i\gamma/2 - \cos k)}{\theta_k^\pm}, \quad r_{xk}^\pm = \frac{2 \sin k}{\theta_k^\pm} \end{aligned} \quad (\text{B2})$$

and we have dropped the subscript s used in the main text indicating square protocol here and for the rest of this section.

The expression of H_{Fk} can be obtained in a straightforward manner. To express this concisely, we define a set of new unit vectors $\vec{n}_k = (n_{xk}, n_{yk}, n_{zk})^T$ which are related to r_{xk}^\pm and r_{zk}^\pm by

This leads to

$$\begin{aligned} E_k^\pm &= \pm \hbar\alpha_k, \quad \psi_k = \begin{pmatrix} u_k^\pm \\ v_k^\pm \end{pmatrix} \\ \begin{pmatrix} u_k^\pm \\ v_k^\pm \end{pmatrix} &= \begin{pmatrix} n_{zk} \pm 1 \\ n_{xk} + i n_{yk} \end{pmatrix} \frac{1}{\sqrt{|n_{zk} \pm 1|^2 + |n_{xk} + i n_{yk}|^2}} \end{aligned} \quad (\text{B5})$$

The wavefunction after n cycles of the drive can therefore be written, in terms of u_k^\pm and v_k^\pm as given in Eq. 12 of the main text. Here we note that the steady state wavefunction corresponds to

$$|\psi_k^{\text{steady}}\rangle = \frac{u_k^{+(-)} + v_k^{+(-)} c_k^\dagger c_{-k}^\dagger |0\rangle}{\sqrt{|u_k^{+(-)}|^2 + |v_k^{+(-)}|^2}} \quad (\text{B6})$$

if $\text{Im}[E_k] = \Gamma_k > 0 (< 0)$. Thus the steady state changes

with sign change of Γ_k . Combining these results, we obtain the final form of the steady states used in the main text

$$|\psi^{\text{steady}}\rangle = \prod_{k>0} \left(u_k^{\text{steady}} |0\rangle + v_k^{\text{steady}} \hat{c}_k^\dagger \hat{c}_{-k}^\dagger |0\rangle \right)$$

$$u_k^{\text{steady}} = \frac{S_{zk} + E_k \text{sgn}(\Gamma_k)}{C_k} \quad v_k^{\text{steady}} = \frac{S_{xk} + iS_{yk}}{C_k}$$

$$S_{jk} = \alpha_k n_{jk} \hbar, \quad C_k = \sqrt{|u_k^{\text{steady}}|^2 + |v_k^{\text{steady}}|^2} \quad (\text{B7})$$

A similar procedure can be carried out for obtaining the steady state corresponding to the continuous drive protocol. However, for such a protocol, analytic expressions for Floquet eigenstates and eigenvalues can not be obtained; in the main text, we have obtained these quantities numerically and used them to obtain the exact steady state wavefunctions.

Appendix C: Szegő's theorem and the absence of volume law scaling

In this appendix, we show the absence of volume law scaling for large ℓ using Szegő's strong limit theorem⁸⁰. We note that this analysis ignores the jump singularities of Π_{xk} that are separately analyzed in Sec. IIB of the main text.

We begin by noting that $\hat{\Pi}_k = (\Pi_{xk}, \Pi_{yk}, \Pi_{zk})$ satisfies

$$\left\| \hat{\Pi}_k \right\|^2 = 1$$

$$\text{Det} \left(\hat{\Pi}_k \right) = - \left\| \hat{\Pi}_k \right\|^2 = -1 \quad (\text{C1})$$

This property follows from the normalization of the driven wavefunction as discussed in Sec. IIB. We also note that the Fourier transform of $\hat{\Pi}(k)$, defined as,

$$\Pi_\ell = \int_{-\pi}^{+\pi} \frac{dk}{2\pi} e^{-ik\ell} \hat{\Pi}(k) \cdot \hat{\sigma} \quad (\text{C2})$$

serves as the elements of the correlation matrix B_ℓ . These elements are matrix valued and in terms of them one obtains

$$G_\ell = \begin{pmatrix} \Pi_0 & \Pi_{-1} & \dots & \Pi_{1-\ell} \\ \Pi_1 & \Pi_0 & \dots & \Pi_{2-\ell} \\ \dots & \dots & \dots & \dots \\ \Pi_{\ell-1} & \Pi_{\ell-2} & \dots & \Pi_0 \end{pmatrix}, \quad (\text{C3})$$

Thus the correlation functions lead to a block Toeplitz matrix.

For later convenience, we next introduce the function $\mathcal{D}_\ell(\lambda)$ given by

$$\mathcal{D}_\ell(\lambda) \equiv \lambda I - G_\ell \quad (\text{C4})$$

where I denotes the identity matrix. In addition, following standard procedure in the literature^{78,79}, we also define the function $e(x, \lambda)$

$$e(x, \lambda) \equiv -\frac{x+\lambda}{2} \ln \frac{x+\lambda}{2} - \frac{x-\lambda}{2} \ln \frac{x-\lambda}{2} \quad (\text{C5})$$

It is well known that in terms of this function the von-Neumann entanglement entropy can be written as $S_\ell = \sum_{m=-\ell}^{\ell} e(1, \nu_m)$ where ν_m denote the eigenvalues of G_ℓ .

Next, we note that from Eq. (C4) we can obtain

$$\text{Det}(\mathcal{D}_\ell(\lambda)) = \prod_{m=1}^{\ell} (\lambda^2 - \nu_m^2) \quad (\text{C6})$$

where we have used the property $\nu_m = -\nu_{-m}$. Using Cauchy's residue theorem and Eq. C6 we can therefore express S_ℓ as a complex integral as

$$S_\ell = \frac{1}{4\pi i} \oint_{\mathcal{C}} d\lambda e(1, \lambda) \frac{d}{d\lambda} \ln [\text{Det}(\mathcal{D}_\ell(\lambda))] \quad (\text{C7})$$

where \mathcal{C} is the contour surrounding the zeros of $\text{Det}[\mathcal{D}_\ell(\lambda)]$.

To obtain the linear term in S_ℓ , we first define

$$\mathcal{A}_k = \lambda I - \hat{\Pi}_k \quad (\text{C8})$$

and use Szegő's strong limit theorem. In the leading order this theorem allows one to write⁸⁰

$$\mathcal{S}_\infty(\ell) \approx \frac{\ell}{8\pi^2 i} \oint_{\mathcal{C}} d\lambda e(1, \lambda) \int_0^{2\pi} dk \frac{d}{d\lambda} \ln [\text{Det}(\mathcal{A}_k)] \quad (\text{C9})$$

Using Eq. C1, we find that $\text{Det}(\mathcal{A}_k) = \lambda^2 - 1$. Using this, Eq. (C9) gives us

$$\begin{aligned} \mathcal{S}_{\text{steady}}(\ell) &\approx \frac{\ell}{8\pi^2 i} \oint_{\mathcal{C}} d\lambda e(1, \lambda) \int_0^{2\pi} dk \frac{d}{d\lambda} [\ln(\lambda - 1) + \ln(\lambda + 1)] \\ &= \frac{\ell}{8\pi^2 i} \oint_{\mathcal{C}} d\lambda e(1, \lambda) \int_0^{2\pi} dk \left[\frac{1}{\lambda - 1} + \frac{1}{\lambda + 1} \right] \\ &= \frac{\ell}{4\pi i} \oint_{\mathcal{C}} d\lambda \left[\frac{e(1, \lambda)}{\lambda - 1} + \frac{e(1, \lambda)}{\lambda + 1} \right] = 0 \end{aligned} \quad (\text{C10})$$

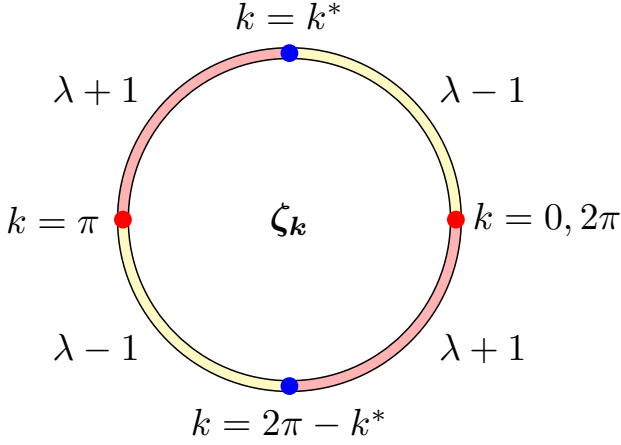


FIG. 8: Schematic representation of the jump singularities which separates the Brillouin zone into different regions. The solution of ζ_k is obtained by equating it to $\lambda \pm 1$ in these regions as schematically shown. See text for details.

where the last line follows from the presence of simple poles at $\lambda = \pm 1$.

Thus we arrive at the conclusion that the coefficient of the linear term vanishes. This indicates that S_ℓ can show either logarithmic dependence on ℓ or lead to an area law behavior (S_ℓ being a constant) for large ℓ . We show in the main text using a Fisher-Hartwig type analysis that the first behavior follows from the jump singularities of Π_{xk} at small γ while the latter behavior is seen at large γ where such jumps are absent.

Appendix D: Fisher-Hartwig singularities of Π_{xk}

In this section, we sketch the derivation of \mathcal{D}_ℓ starting from the expression of $\Pi_{xk}^{(1)}$ (Eq. 19) in the main text. We are going to first sketch this derivation for $\delta = 1$ where the norm of Π_{xk} is unity. In the rest of the appendix, we shall shift the Brillouin zone from $0 \leq k \leq 2\pi$ instead of $-\pi \leq k \leq \pi$. The singularities therefore occur at $k = k^*$ and $2\pi - k^*$. This allows us to write

$$\begin{aligned} \tilde{\Pi}_k^{(1)} &= g(k) \sigma^x \quad 0 \leq k < 2\pi \\ \zeta_k &= \lambda - g(k) \end{aligned} \quad (\text{D1})$$

where $g(k) = \pm 1$. We perform the calculations in the standard form by working on the unit circle S^1 : $z = e^{ik}$. The generator, $\zeta(z)$ contains Fisher-Hartwig jump singularities as shown schematically in Fig. 8; hence one can apply the Fisher-Hartwig conjecture to find the asymptotic value of the Toeplitz determinant $\mathcal{D}_\ell(\lambda)$ which in turn will allow us to obtain the asymptotic analytic form of S_ℓ .

To this end, we express the generator $\zeta(z)$ in the Fisher-Hartwig form. We denote $z_j = e^{ik_j}$, where $k_j = 0, k^*, \pi, (2\pi - k^*)$, leading to $z_j = 1, z^*, -1, 1/z^*$, where

$z^* = \exp[ik^*]$, to be the positions of the jump discontinuities. We note that the discontinuities at $z = \pm 1$ are spurious as explained in the main text. We divide the unit circle S^1 in four regions as shown in Fig. 8. In each region, the generator $\zeta(z)$ has a constant value $\lambda \pm 1$.

We also define $g_{z_j\beta_j}(z)$ for $j = 1, 2, 3$ that changes across the discontinuity points and $g_{z_0\beta_0}$ which remains the same over the entire unit circle; this allows us to choose $g_{z_0\beta_0} = \exp[-i\pi\beta_0]$. The other $g_{z_j\beta_j}(z)$ has the following structure.

$$\begin{aligned} g_{z_j\beta_j}(z) &= e^{-i\pi\beta_j} \quad 0 < k < k_j \\ &= e^{i\pi\beta_j} \quad k_j < k < 2\pi \end{aligned} \quad (\text{D2})$$

In terms of this function the generator takes the following form

$$\begin{aligned} \zeta(z) &= e^{V(z)} \left(\frac{z}{z_0}\right)^{\beta_0} \left(\frac{z}{z_1}\right)^{\beta_1} \left(\frac{z}{z_2}\right)^{\beta_2} \left(\frac{z}{z_3}\right)^{\beta_3} \\ &\times e^{-i\pi\beta_0} g_{z_1\beta_1}(z) g_{z_2\beta_2}(z) g_{z_3\beta_3}(z) \end{aligned} \quad (\text{D3})$$

In order to find the functional form of the functions $g_{z_j\beta_j}(z)$, one needs to solve a set of coupled equations. It is clear from Fig. 8 that the condition $\zeta(z) = \lambda \pm 1$ necessitates $V(z) = \ln \eta_0(\lambda)$ to be independent of z and

$$\beta_0 + \beta_1 + \beta_2 + \beta_3 = 0 \quad (\text{D4})$$

With these conditions the generator takes the following form

$$\zeta(z) = \eta_0(\lambda) \prod_{j=1}^3 z_j^{\beta_j} e^{-i\pi\beta_0} g_{z_1\beta_1}(z) g_{z_2\beta_2}(z) g_{z_3\beta_3}(z) \quad (\text{D5})$$

With this form of $\zeta(z)$, we now seek the solution of the equations

$$\zeta(z) = \lambda \pm 1 \quad (\text{D6})$$

as shown schematically in Fig. 8. The solutions of these equations are straightforward and yield

$$\begin{aligned} \beta_0 &= \beta_2 = \frac{1}{2\pi i} \ln \left(\frac{\lambda + 1}{\lambda - 1} \right) \\ \beta_1 &= \beta_3 = \frac{1}{2\pi i} \ln \left(\frac{\lambda - 1}{\lambda + 1} \right) \\ \eta_0(\lambda) &= \sqrt{\lambda^2 - 1} \end{aligned} \quad (\text{D7})$$

The above solution above is for $\text{Sgn}(\tilde{h}_1 f(T)) = 1$. Solution for $\text{Sgn}(\tilde{h}_1 f(T)) = -1$ can be obtained by exchanging $\lambda + 1$ and $\lambda - 1$. The final expression of S_ℓ will remain the same in both cases.

The form of $\zeta(z)$ (Eq. D6) obtained allows us to write the matrix $G_\ell = B_\ell \otimes \sigma^x$, where B_ℓ is given by Eq. 20 in the main text. To this end, we define

$$\mathcal{D}_\ell(\lambda) = \mathbb{1}_{2\ell \times 2\ell} - G_\ell \quad (\text{D8})$$

where G_ℓ is a $2\ell \times 2\ell$ Toeplitz matrix. As all the non-trivial correlations are embedded within the $\ell \times \ell$ Toeplitz matrix B_ℓ , we compute the asymptotics of $\text{Det}[\tilde{\mathcal{D}}_\ell(\lambda)]$ in order to obtain the relevant information about the entanglement entropy of the system, where

$$\tilde{\mathcal{D}}_\ell(\lambda) = \lambda \mathbb{1}_{\ell \times \ell} - B_\ell. \quad (\text{D9})$$

Following the Fisher-Hartwig conjecture, we can write

$$\text{Det}(\tilde{\mathcal{D}}_\ell(\lambda)) = (F[\eta(\lambda)])^\ell \ell^{-\sum_{i=0}^3 \beta_i^2(\lambda)} \tilde{E} \quad (\text{D10})$$

where $F[\eta(\lambda)] = \eta_0(\lambda)$ and \tilde{E} can be expressed in terms of Barnes G function^{78,79} whose form is not important for our analysis as long as we only restrict ourselves to the leading order contribution to S_ℓ . This allows one to write

$$\begin{aligned} \ln(\text{Det}(\mathcal{D}_\ell(\lambda))) &= 2 \ln(\text{Det}(\tilde{\mathcal{D}}_\ell(\lambda))) \\ &= 2[\ell \ln(F[\eta(\lambda)]) - \sum_{i=1,3} \beta_i^2(\lambda) \ln(\ell)] \\ &\quad + \text{sub-leading corrections} \end{aligned} \quad (\text{D11})$$

The first term, which arises from non-singular part of ζ_k , does not contribute to S_ℓ . This is seen by application of Szegő's theorem and is detailed in App. C. In the rest of this section, we shall be concerned with the term $\sim \ln \ell$ in Eq. D11. Note that we have omitted the contribution of β_0 and β_2 ; this amounts to subtracting out the contribution from the spurious singularities at $k = 0, \pi$.

The above mentioned calculation may be easily repeated with $\delta \neq 1$. A procedure, exactly similar to the one outlined above, requires solution of the equations $\zeta_k = \lambda \pm \delta$ and yields

$$\begin{aligned} \beta_0 &= \beta_2 = \frac{1}{2\pi i} \ln \left(\frac{\lambda + \delta}{\lambda - \delta} \right) \\ \beta_1 &= \beta_3 = \frac{1}{2\pi i} \ln \left(\frac{\lambda - \delta}{\lambda + \delta} \right) \\ \eta_0(\lambda) &= \sqrt{\lambda^2 - \delta^2} \end{aligned} \quad (\text{D12})$$

Substituting Eq. D12 in Eq. D11, one finally gets the expression of $\ln[\text{Det}(\mathcal{D}_\ell)]$ used in Eq. 21 in the main text.

-
- ¹ J. Eisert, M. Cramer, and M. B. Plenio, Rev. Mod. Phys. **82**, 277 (2010).
² L. Amico, R. Fazio, A. Osterloh, and V. Vedral, Rev. Mod. Phys. **80**, 517 (2008).
³ P. Calabrese and J. Cardy, J. Stat. Mech. **6**, 06002 (2004); R. Ghosh, N. Dupuis, A. Sen, and K. Sengupta, Phys. Rev. B **101**, 245130 (2020).
⁴ S. Ryu and T. Takayanagi, Phys. Rev. Lett. **96**, 181602 (2006).
⁵ M. B. Hastings, J. Stat. Mech. **2007** P0802 (2007).
⁶ P. Calabrese and J. Cardy, J. Stat. Mech. **7** 04010 (2005); I. Peschel, J. Phys. A **36**, L205 (2003); I. Peschel and V. Eisler, J. Phys. A: Math. Theor. **42**, 504003 (2009); S-A Cheong and C.L. Henley, Phys. Rev. B **69**, 075111 (2004).
⁷ R. N. C. Pfeifer, G. Evenbly, G. Vidal, Phys. Rev. A **79**, 040301(R) (2009).
⁸ A. Polkovnikov, K. Sengupta, A. Silva, and M. Vengalattore, Rev. Mod. Phys. **83**, 863 (2011).
⁹ D. Ziarmaga, Adv. Phys. **59**, 1063 (2010).
¹⁰ A. Dutta, G. Aeppli, B. K. Chakrabarti, U. Divakaran, T. F. Rosenbaum, and D. Sen, *Quantum phase transitions in transverse field spin models: from statistical physics to quantum information* (Cambridge University Press, Cambridge, 2015).
¹¹ S. Mondal, D. Sen, and K. Sengupta, *Quantum Quenching, Annealing and Computation*, edited by A. Das, A. Chandra, and B. K. Chakrabarti, Lecture Notes in Physics **802**, 21 (Springer, Berlin, Heidelberg, 2010); C. De Grandi and A. Polkovnikov, *ibid.*, **802**, 75.
¹² A. del Campo and K. Sengupta, Eur. Phys. J. Special Topics **224**, 189 (2015).
¹³ M. Bukov, L. D'Alessio and A. Polkovnikov, Advances in Physics **64**, 139 (2015).
¹⁴ S. Blanes, F. Casas, J. A. Oteo, and J. Ros, Physics Reports **470**, 151 (2009).
¹⁵ L. D'Alessio and A. Polkovnikov, Ann. Phys. **333**, 19 (2013).
¹⁶ L. D'Alessio, Y. Kafri, A. Polokovnikov, and M. Rigol, Adv. Phys. **65**, 239 (2016).
¹⁷ A. Sen, D. Sen, and K. Sengupta, J. Phys. Cond. Mat. **33**, 443003 (2021).
¹⁸ I. Bloch, J. Dalibard, and W. Zwerger, Rev. Mod. Phys. **80**, 885 (2008).
¹⁹ M. Greiner, O. Mandel, T. Esslinger, T. W. Hansch, and I. Bloch, Nature **39**, 415 (2002).
²⁰ J. Simon, W. S. Bakr, R. Ma, M. E. Tai, P. M. Preiss, and M. Greiner, Nature (London) **472**, 307 (2011).
²¹ W. Bakr, A. Peng, E. Tai, R. Ma, J. Simon, J. Gillen, S. Foelling, L. Pollet, and M. Greiner, Science **329**, 547 (2010).
²² H. Bernien, S. Schwartz, A. Keesling, H. Levine, A. Omran, H. Pichler, S. Choi, A. S. Zibrov, M. Endres, M. Greiner, V. Vuletic, and M. D. Lukin, Nature **551**, 579 (2017).
²³ V. Khemani, A. Lazarides, R. Moessner, and S. L. Sondhi, Phys. Rev. Lett. **116**, 250401 (2016).
²⁴ D. V. Else, B. Bauer, and C. Nayak, Phys. Rev. Lett. **117**, 090402 (2016).
²⁵ J. Zhang, P. W. Hess, A. Kyprianidis, P. Becker, A. Lee, J. Smith, G. Pagano, I-D. Potirniche, A. C. Potter, A. Vishwanath, N. Y. Yao, and C. Monroe, Nature (London) **543**, 217 (2017).
²⁶ A. Das, Phys. Rev. B **82**, 172402 (2010).
²⁷ S. Bhattacharyya, A. Das, and S. Dasgupta, Phys. Rev. B **86** 054410 (2010).
²⁸ S. Hegde, H. Katiyar, T. S. Mahesh, and A. Das, Phys. Rev. B **90**, 174407 (2014).
²⁹ S. Mondal, D. Pekker, and K. Sengupta, Europhys. Lett.

- 100**, 60007 (2012).
- ³⁰ U. Divakaran and K. Sengupta, Phys. Rev. B **90**, 184303 (2014).
- ³¹ T. Nag, S. Roy, A. Dutta, and D. Sen, Phys. Rev. B **89**, 165425 (2014); T. Nag, D. Sen, and A. Dutta, Phys. Rev. A **91**, 063607 (2015).
- ³² A. Agarwala, U. Bhattacharya, A. Dutta, and D. Sen, Phys. Rev. B **93**, 174301 (2016); A. Agarwala and D. Sen, Phys. Rev. B **95**, 014305 (2017).
- ³³ D. J. Luitz, Y. Bar Lev, and A. Lazarides, SciPost Phys. **3**, 029 (2017); D. J. Luitz, A. Lazarides, and Y. Bar Lev, Phys. Rev. B **97**, 020303 (2018).
- ³⁴ T. Oka and H. Aoki, Phys. Rev. B **79**, 081406 (R) (2009).
- ³⁵ T. Kitagawa, E. Berg, M. Rudner, and E. Demler, Phys. Rev. B **82**, 235114 (2010); N. H. Lindner, G. Refael, and V. Galitski, Nat. Phys. **7**, 490 (2011).
- ³⁶ T. Kitagawa, T. Oka, A. Brataas, L. Fu, and E. Demler, Phys. Rev. B **84**, 235108 (2011); B. Mukherjee, P. Mohan, D. Sen, and K. Sengupta, Phys. Rev. B **97**, 205415 (2018).
- ³⁷ M. Thakurathi, A. A. Patel, D. Sen, and A. Dutta, Phys. Rev. B **88**, 155133 (2013); A. Kundu, H. A. Fertig, and B. Seradjeh, Phys. Rev. Lett. **113**, 236803 (2014); M. Thakurathi, K. Sengupta, and D. Sen Physical Review B **89**, 235434 (2014).
- ³⁸ F. Nathan and M. S. Rudner, New J. Phys. **17**, 125014 (2015); B. Mukherjee, A. Sen, D. Sen, and K. Sengupta, Phys. Rev. B **94**, 155122 (2016).
- ³⁹ M. Heyl, A. Polkovnikov, and S. Kehrein, Phys. Rev. Lett. **110**, 135704 (2013); For a review, see M. Heyl, Rep. Prog. Phys. **81**, 054001 (2018).
- ⁴⁰ A. Sen, S. Nandy, and K. Sengupta, Phys. Rev. B **94**, 214301 (2016); S. Nandy, K. Sengupta, and A. Sen, J. Phys. A: Math. Theor. **51**, 334002 (2018); M. Sarkar and K. Sengupta, Phys. Rev. B **102**, 235154 (2020).
- ⁴¹ S. Aditya, S. Samanta, A. Sen, K. Sengupta, and D. Sen, arXiv:2112.02915 (unpublished); A. A. Makki, S. Bandyopadhyay, S. Maity, and A. Dutta, arXiv:2112.02930 (unpublished); S.E. Tapias Arze, P. W. Clayes, I. P. Castillo, and J-S Caux, SciPost Phys. Core **3**, 001 (2020).
- ⁴² B. Mukherjee, S. Nandy, A. Sen, D. Sen and K. Sengupta, Phys. Rev. B **101**, 245107 (2020)
- ⁴³ B. Mukherjee, A. Sen, D. Sen and K. Sengupta, Phys. Rev. B **102**, 075123 (2020).
- ⁴⁴ B. Mukherjee, A. Sen, and K. Sengupta, Phys. Rev. B **106**, 064305 (2022).
- ⁴⁵ S. Ghosh, I. Paul, and K. Sengupta, Phys. Rev. Lett. **130**, 120401 (2023).
- ⁴⁶ For a recent review of non-Hermitian topological phenomena, see N. Okuma and M. Sato, arXiv:2205.10379 (unpublished).
- ⁴⁷ J. Gonzalez and R. A. Molina, Phys. Rev. B **96**, 045437 (2017); V. Kozii and L. Fu, arXiv:1708.05841 (unpublished); A. A. Zyuzin and A. Y. Zyuzin, Phys. Rev. B **97**, 041203(R) (2018); H. Shen and L. Fu, Phys. Rev. Lett. **121**, 026403 (2018); R. A. Molina and J. Gonzalez, Phys. Rev. Lett. **120**, 146601 (2018); T. Yoshida, R. Peters, and N. Kawakami, Phys. Rev. B **98**, 035141 (2018); J. Carlstrom and E. J. Bergholtz, Phys. Rev. A **98**, 042114 (2018).
- ⁴⁸ T. M. Philip, M. R. Hirsbrunner, and M. J. Gilbert, Phys. Rev. B **98**, 155430 (2018); Y. Chen and H. Zhai, Phys. Rev. B **98**, 245130 (2018); K. Moors, A. A. Zyuzin, A. Y. Zyuzin, R. P. Tiwari, and T. L. Schmidt, Phys. Rev. B **99**, 041116(R) (2018); R. Okugawa and T. Yokoyama, Phys. Rev. B **99**, 041202(R) (2019); J. C. Budich, J. Carlstrom, F. K. Kunst, and E. J. Bergholtz, Phys. Rev. B **99**, 041406(R) (2019).
- ⁴⁹ Z. Yang and J. Hu, Phys. Rev. B **99**, 081102(R) (2019); T. Yoshida, R. Peters, N. Kawakami, and Y. Hatsugai, Phys. Rev. B **99**, 121101(R) (2019); Y. Wu, W. Liu, J. Geng, X. Song, X. Ye, C.-K. Duan, X. Rong, and J. Du, Science **364**, 878 (2019); P. San-Jose, J. Cayao, E. Prada, and R. Aguado, Sci. Rep. **6**, 21427 (2016); Q.-B. Zeng, B. Zhu, S. Chen, L. You, and R. Lu, Phys. Rev. A **94**, 022119 (2016); C. Li, X. Z. Zhang, G. Zhang, and Z. Song, Phys. Rev. B **97**, 115436 (2018); J. Cayao and A. M. Black-Schaffer Phys. Rev. B **105**, 094502 (2022); R. Arouca, J. Cayao, A. M. Black-Schaffer, arXiv:2206.15324 (unpublished).
- ⁵⁰ K. Kawabata, Y. Ashida, H. Katsura, and M. Ueda, Phys. Rev. B **98**, 085116 (2018); A. Guo, G. J. Salamo, D. Duchesne, R. Morandotti, M. Volatier-Ravat, V. Aimez, G. A. Siviloglou, and D. N. Christodoulides, Phys. Rev. Lett. **103**, 093902 (2009); C. E. Ruter, K. G. Makris, R. El-Ganainy, D. N. Christodoulides, M. Segev, and D. Kip, Nat. Phys. **6**, 192 (2010); L. Feng, M. Ayache, J. Huang, Y.-L. Xu, M.-H. Lu, Y.-F. Chen, Y. Fainman, and A. Scherer, Science **333**, 729 (2011); A. Regensburger, C. Bersch, M.-A. Miri, G. Onishchukov, D. N. Christodoulides, and U. Peschel, Nature (London) **488**, 167 (2012).
- ⁵¹ L. Feng, Y.-L. Xu, W. S. Fegadolli, M.-H. Lu, J. E. Oliveira, V. R. Almeida, Y.-F. Chen, and A. Scherer, Nat. Mater. **12**, 108 (2013); C. Poli, M. Bellec, U. Kuhl, F. Mortessagne, and H. Schomerus, Nat. Commun. **6**, 6710 (2015); B. Zhen, C.W. Hsu, Y. Igarashi, L. Lu, I. Kaminer, A. Pick, S.-L. Chua, J. D. Joannopoulos, and M. Solja.i., Nature (London) **525**, 354 (2015); H. Zhao, S. Longhi, and L. Feng, Sci. Rep. **5**, 17022 (2015); K. Ding, Z. Q. Zhang, and C. T. Chan, Phys. Rev. B **92**, 235310 (2015).
- ⁵² S. Weimann, M. Kremer, Y. Plotnik, Y. Lumer, S. Nolte, K. Makris, M. Segev, M. Rechtsman, and A. Szameit, Nat. Mater. **16**, 433 (2017); H. Hodaei, A. U. Hassan, S. Wittek, H. Garcia-Gracia, R. El-Ganainy, D. N. Christodoulides, and M. Khajavikhan, Nature (London) **548**, 187 (2017); W. Chen, K. Ozdemir, G. Zhao, J. Wiersig, and L. Yang, Nature (London) **548**, 192 (2017); P. St-Jean, V. Goblot, E. Galopin, A. Lemaitre, T. Ozawa, L. Le Gratiet, I. Sagnes, J. Bloch, and A. Amo, Nat. Photonics **11**, 651 (2017).
- ⁵³ B. Bahari, A. Ndao, F. Vallini, A. E. Amili, Y. Fainman, and B. K. Le, Science **358**, 636 (2017); J. Wang, H. Y. Dong, Q. Y. Shi, W. Wang, and K. H. Fung, Phys. Rev. B **97**, 014428 (2018); H. Zhou, C. Peng, Y. Yoon, C.W. Hsu, K. A. Nelson, L. Fu, J. D. Joannopoulos, M. Solja.i., and B. Zhen, Science **359**, 1009 (2018); M. Parto, S. Wittek, H. Hodaei, G. Harari, M. A. Bandres, J. Ren, M. C. Rechtsman, M. Segev, D. N. Christodoulides, and M. Khajavikhan, Phys. Rev. Lett. **120**, 113901 (2018); H. Zhao, P. Miao, M. H. Teimourpour, S. Malzard, R. El-Ganainy, H. Schomerus, and L. Feng, Nat. Commun. **9**, 981 (2018).
- ⁵⁴ G. Harari, M. A. Bandres, Y. Lumer, M. C. Rechtsman, Y. D. Chong, M. Khajavikhan, D. N. Christodoulides, and M. Segev, Science **359**, 1230 (2018); M. A. Bandres, S. Wittek, G. Harari, M. Parto, J. Ren, M. Segev, D. N. Christodoulides, and M. Khajavikhan, Science **359**, 1231 (2018); M. Pan, H. Zhao, P. Miao, S. Longhi, and L. Feng, Nat. Commun. **9**, 1308 (2018); L. Jin and Z. Song, Phys. Rev. Lett. **121**, 073901 (2018); S. Malzard and H. Schome-

- rus, Phys. Rev. A **98**, 033807 (2018); Z. Oztas and C. Yuce, Phys. Rev. A **98**, 042104 (2018).
- ⁵⁵ M. Kremer, T. Biesenthal, L. J. Maczewsky, M. Heinrich, R. Thomale, and A. Szameit, Nat. Commun. **10**, 435 (2019); K. Y. Bliokh, D. Leykam, M. Lein, and F. Nori, Nat. Commun. **10**, 580 (2019); S. Wang, B. Hou, W. Lu, Y. Chen, Z. Zhang, and C. Chan, Nat. Commun. **10**, 832 (2019); S. Chen, W. Zhang, B. Yang, T. Wu, and X. Zhang, Sci. Rep. **9**, 5551 (2019); T. E. Lee and C.-K. Chan, Phys. Rev. X **4**, 041001 (2014); Y. Xu, S.-T. Wang, and L.-M. Duan, Phys. Rev. Lett. **118**, 045701 (2017); Y. Ashida, S. Furukawa, and M. Ueda, Nat. Commun. **8**, 15791 (2017); Z. Gong, Y. Ashida, K. Kawabata, K. Takasan, S. Higashikawa, and M. Ueda, Phys. Rev. X **8**, 031079 (2018); M. Nakagawa, N. Kawakami, and M. Ueda, Phys. Rev. Lett. **121**, 203001 (2018); K. Takata and M. Notomi, Phys. Rev. Lett. **121**, 213902 (2018); L. Pan, S. Chen, and X. Cui, Phys. Rev. A **99**, 011601(R) (2019).
- ⁵⁶ J. Li, A. K. Harter, J. Liu, L. de Melo, Y. N. Joglekar, and L. Luo, Nat. Commun. **10**, 855 (2019); T. Liu, Y.-R. Zhang, Q. Ai, Z. Gong, K. Kawabata, M. Ueda, and F. Nori, Phys. Rev. Lett. **122**, 076801 (2019); M. S. Rudner and L. S. Levitov, Phys. Rev. Lett. **102**, 065703 (2009); J. M. Zeuner, M. C. Rechtsman, Y. Plotnik, Y. Lumer, S. Nolte, M. S. Rudner, M. Segev, and A. Szameit, Phys. Rev. Lett. **115**, 040402 (2015); K. Mochizuki, D. Kim, and H. Obuse, Phys. Rev. A **93**, 062116 (2016); L. Xiao, X. Zhan, Z. Bian, K. Wang, X. Zhang, X. Wang, J. Li, K. Mochizuki, D. Kim, N. Kawakami et al., Nat. Phys. **13**, 1117 (2017).
- ⁵⁷ N. Hatano and D. R. Nelson, Phys. Rev. Lett. **77**, 570 (1996); N. Hatano and D. R. Nelson, Phys. Rev. B **56**, 8651 (1997); N. Hatano and D. R. Nelson, Phys. Rev. B **58**, 8384 (1998).
- ⁵⁸ J. A. S. Lourenco, R. L. Eneias, and R. G. Pereira, Phys. Rev. B **98**, 085126 (2018); E. I. Rosenthal, N. K. Ehrlich, M. S. Rudner, A. P. Higginbotham, and K. W. Lehnert, Phys. Rev. B **97**, 220301(R) (2018); M. Wang, L. Ye, J. Christensen, and Z. Liu, Phys. Rev. Lett. **120**, 246601 (2018).
- ⁵⁹ M. Ezawa, Phys. Rev. B **99**, 121411(R) (2019); M. Ezawa, Phys. Rev. B **99**, 201411(R) (2019); M. Ezawa, Phys. Rev. B **100**, 045407 (2019); M. Prasad, H. K. Yadalam, C. Aron, and M. Kulkarni Phys. Rev. A **105**, L050201 (2022).
- ⁶⁰ J.-J. Liu, Z.-W. Li, Z.-G. Chen, W. Tang, A. Chen, B. Liang, G. Ma, and J.-C. Cheng Phys. Rev. Lett. **129**, 084301 (2022); W. Tang, K. Ding, and G. Ma, National Science Review **9**, 1 (2022).
- ⁶¹ J. Dalibard, Y. Castin, and K. Molmer, Phys. Rev. Lett. **68**, 580 (1992).
- ⁶² A. J. Daley, Adv. Phys. **63**, 77 (2014).
- ⁶³ Y. C. Hu and T. L. Hughes, Phys. Rev. B **84**, 153101 (2011); K. Esaki, M. Sato, K. Hasebe, and M. Kohmoto, Phys. Rev. B **84**, 205128 (2011); T. E. Lee, Phys. Rev. Lett. **116**, 133903 (2016); D. Leykam, K. Y. Bliokh, C. Huang, Y. D. Chong, and F. Nori, Phys. Rev. Lett. **118**, 040401 (2017); V. M. Martinez Alvarez, J. E. Barrios Vargas, and L. E. F. Foa Torres, Phys. Rev. B **97**, 121401(R) (2018); Y. Xiong, J. Phys. Commun. **2**, 035043 (2018); H. Shen, B. Zhen, and L. Fu, Phys. Rev. Lett. **120**, 146402 (2018).
- ⁶⁴ C. Yuce, Phys. Rev. A **97**, 042118 (2018); C. Yin, H. Jiang, L. Li, R. Lu, and S. Chen, Phys. Rev. A **97**, 052115 (2018); C. Yuce, Phys. Rev. A **98**, 012111 (2018); F. K. Kunst, E. Edvardsson, J. C. Budich, and E. J. Bergholtz, Phys. Rev. Lett. **121**, 026808 (2018); S. Yao and Z. Wang, Phys. Rev. Lett. **121**, 086803 (2018); S. Yao, F. Song, and Z. Wang, Phys. Rev. Lett. **121**, 136802 (2018); K. Kawabata, K. Shiozaki, and M. Ueda, Phys. Rev. B **98**, 165148 (2018); C. Yuce and Z. Oztas, Sci. Rep. **8**, 17416 (2018).
- ⁶⁵ K. Kawabata, S. Higashikawa, Z. Gong, Y. Ashida, and M. Ueda, Nat. Commun. **10**, 297 (2019); L. Jin and Z. Song, Phys. Rev. B **99**, 081103(R) (2019); H. Wang, J. Ruan, and H. Zhang, Phys. Rev. B **99**, 075130 (2019); D. S. Borgnia, A. J. Kruchkov, and R.-J. Slager, Phys. Rev. Lett. **124**, 056802 (2020); Z. Ozcakmakli Turker and C. Yuce, Phys. Rev. A **99**, 022127 (2019); E. Edvardsson, F. K. Kunst, and E. J. Bergholtz, Phys. Rev. B **99**, 081302(R) (2019).
- ⁶⁶ C.-H. Liu, H. Jiang, and S. Chen, Phys. Rev. B **99**, 125103 (2019); C. H. Lee and R. Thomale, Phys. Rev. B **99**, 201103(R) (2019); F. K. Kunst and V. Dwivedi, Phys. Rev. B **99**, 245116 (2019); K. Yokomizo and S. Murakami, Phys. Rev. Lett. **123**, 066404 (2019).
- ⁶⁷ R. Nehra, and D. Roy, Phys. Rev. B **105**, 195407 (2022); S. Ghosh, I. Paul, and K. Sengupta, arXiv:2307.05679 (unpublished); K. Kawabata, K. Shiozaki, and S. Ryu, Phys. Rev. B **105**, 165137 (2022); K. Yang, D. Vargias, E. J. Bergholtz, S. Morampudi, and F. Wilczek, arXiv:2202.04435 (unpublished).
- ⁶⁸ E. Lee, H. Lee, and B.-J. Yang, Phys. Rev. B **101**, 121109 (2020); S. Mu, C. H. Lee, L. Li, and J. Gong, Phys. Rev. B **102**, 081115 (2020); D.-W. Zhang, Y.-L. Chen, G.-Q. Zhang, L.-J. Lang, Z. Li, and S.-L. Zhu, Phys. Rev. B **101**, 235150 (2020); T. Liu, J. J. He, T. Yoshida, Z.-L. Xiang, and F. Nori, Phys. Rev. B **102**, 235151 (2020).
- ⁶⁹ A. Panda and S. Banerjee, Phys. Rev. B **101**, 184201 (2020); N. Okuma and M. Sato, Phys. Rev. Lett. **126**, 176601 (2021); T. Yoshida, Phys. Rev. B **103**, 125145 (2021); K. Cao, Q. Du, X.-R. Wang, and S.-P. Kou, arXiv:2109.03690 (unpublished); F. Alsallom, L. Herviou, O. V. Yazyev, and M. Brzezinska, arXiv:2110.13164 (unpublished).
- ⁷⁰ S.-B. Zhang, M. M. Denner, Tomas Bzdusek, M. A. Sentef, and T. Neupert, Phys. Rev. B **106**, L121102 (2022).
- ⁷¹ L. Zhou, Q.-h. Wang, H. Wang, and J. Gong, Phys. Rev. A **98**, 022129 (2018); L. Zhou and Q. Du, New J. Phys. **23**, 063041 (2021); B. Zhu, Y. Ke, H. Zhong, and C. Lee, Phys. Rev. Research **2**, 023043 (2020); L. Zhou and J. Gong, Phys. Rev. B **98**, 205417 (2018); L. Zhou, Phys. Rev. B **100**, 184314 (2019); L. Zhou, Y. Gu, and J. Gong, Phys. Rev. B **103**, L041404 (2021).
- ⁷² L. Zhou and W. Han, Phys. Rev. B **106**, 054307 (2022); C.-H. Liu, H. Hu, and S. Chen, Phys. Rev. B **105**, 214305 (2022); L. Zhou, R. W. Bomantara, and S. Wu, SciPost Phys. **13**, 015 (2022).
- ⁷³ S. Zamani, R. Jafari, and A. Langari, Phys. Rev. B **102**, 144306 (2020); R. Jafari and A. Akbari, Phys. Rev. A **103**, 012204 (2021); K. Yang, L. Zhou, W. Ma, X. Kong, P. Wang, X. Qin, X. Rong, Y. Wang, F. Shi, J. Gong, and J. Du, Phys. Rev. B **100**, 085308 (2019); D. Chowdhury, A. Banerjee, and A. Narayan Phys. Rev. A **103**, L051101 (2021).
- ⁷⁴ P. He and Z.-H. Huang, Phys. Rev. A **102**, 062201 (2020); S. Longhi, J. Phys. A: Math. Theor. **50**, 505201 (2017).
- ⁷⁵ X. Turkeshi and M. Schiro, Phys. Rev. B **107**, L020403 (2023).
- ⁷⁶ T. Banerjee and K. Sengupta, Phys. Rev. B **107**, 155117 (2023).
- ⁷⁷ M. E. Fisher and R. E. Hartwig, Adv. Chem. Phys. **15**,

- 333 (1968).
- ⁷⁸ E. L. Basor and C. A. Tracy, *Physica A* **177**, 167 (1991); A. Bottcher, *Jour. Stat. Phys.* **78**, 575 (1995); P. Deift, A. Its, and I. Krasovsky, *Ann. Math.* **174**, 1243 (2011).
- ⁷⁹ A. R. Its, B-Q Jin, and V. E. Korepin, *J. Phys. A: Math.* **38**, 2975 (2005); *ibid*, arXiv:0606178 (unpublished).
- ⁸⁰ G. Szego, *Math. Ann* **76**, 490 (1915); E. Basor, *A Brief History of the Strong Szegő Limit Theorem*, **222**, 73, Eds. H. Dym, M. de Oliveira, and M. Putinar, *Mathematical Methods in Systems, Optimization, and Control, Operator Theory: Advances and Applications* (Springer, Basel 2012).